Thermoplastic Bonding of Microfluidic Substrates

by

Benjamin Michael Judge

S.B. Mechanical Engineering (2011)
Massachusetts Institute of Technology

Submitted to the Department of Mechanical Engineering
in partial fulfillment of the requirements for the degree of

Master of Engineering in Mechanical Engineering

at the

MASSACHUSETTS INSTITUTE OF TECHNOLOGY

September 2012

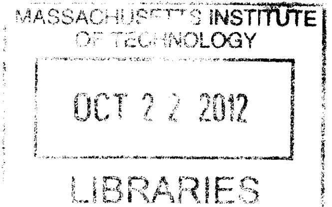

© Benjamin Michael Judge, MMXII. All rights reserved.

The author hereby grants to MIT permission to reproduce and
distribute publicly paper and electronic copies of this thesis document
in whole or in part.

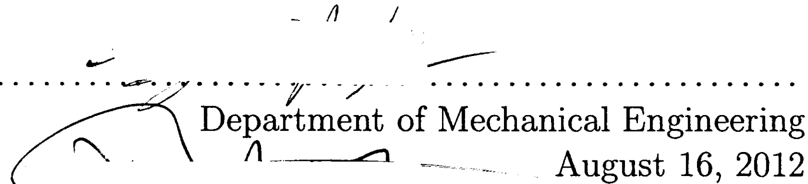

Author ....
Department of Mechanical Engineering
August 16, 2012

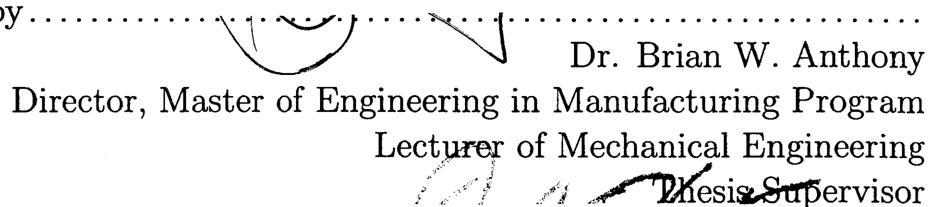

Certified by ....
Dr. Brian W. Anthony
Director, Master of Engineering in Manufacturing Program
Lecturer of Mechanical Engineering
Thesis Supervisor

Accepted by ....
Prof. David E. Hardt
Ralph E. and Eloise F. Cross Professor of Mechanical Engineering
MST Program Co-Chair

Thermoplastic Bonding of Microfluidic Substrates

by

Benjamin Michael Judge

Submitted to the Department of Mechanical Engineering
on August 16, 2012, in partial fulfillment of the
requirements for the degree of
Master of Engineering in Mechanical Engineering

Abstract

The assembly of microfluidic components for lab on a chip (LOC) applications that are manufactured from commodity thermoplastics is challenging. A survey of plastic welding techniques validates that contour transmission laser welding is the most viable and commercially demonstrated option for flexibility and sensitive microfluidic tolerances. However, understanding laser energy transmission and absorption phenomenon further complicates analyzing microfluidic thermoplastic welding, since the instantaneous material properties vary with both temperature and pressure. Thermoplastic welding has steep thermal gradients due to high thermal resistances, resulting in asymmetric heat affected zones (HAZ). Welding fixture sensitivities may be engineered to tune the weld energy required and a desired HAZ bias to reduce microfluidic channel deformation. Energy imparted by resistively heating thin implants can be easily measured and observed. Resistive heating of implants was demonstrated as a low energy, parallel, and feasible microfluidic welding assembly process. Lessons from implant heating can be applied to more complicated but analogous processes.

Thesis Supervisor: Dr. Brian W. Anthony
Director, Master of Engineering in Manufacturing Program
Title: Lecturer of Mechanical Engineering

Contents

1 Introduction **15**

1.1 Company Background 15

1.2 A Global Health Need 16

1.2.1 HIV & AIDS 16

1.2.2 Point-of-Care Diagnostics 17

1.3 LOC to POC 18

1.3.1 Microfluidics 18

1.3.2 Advantages 18

1.3.3 Industry Note 19

1.4 Product Development 20

1.4.1 Cell Chromatography 20

1.4.2 Electrochemical Sensing 20

1.4.3 Pressing Challenges 21

1.5 The MEng Capstone Project 22

1.6 Thesis Overview 22

1.7 Focus of Thesis 23

2 Cuvette Assembly **25**

2.1 Material Selection 25

2.2 Cuvette Assembly 27

2.3 Assembly Issues 27

2.4 Functional Requirements 28

2.4.1 Geometric Dimensioning and Tolerancing 29

2.4.2 Fluid Dynamics 29
2.4.3 System Performance 30
2.4.4 Design for Manufacturing 31
2.4.5 Design for R&D 31
2.5 LOC Industry Context 32

3 Thermoplastic Welding Survey **33**
3.1 Bonding Classification 33
3.1.1 Solvent 34
3.2 Welding with an External Heat Source 34
3.2.1 Hot Gas 35
3.2.2 Hot Plate 35
3.2.3 Hot Bar and Impulse 36
3.3 Welding via Mechanical Movement 37
3.3.1 Spin 38
3.3.2 Vibration 38
3.3.3 Ultrasonic 38
3.4 Welding with Electromagnetism 39
3.4.1 Resistive Implant 40
3.4.2 Induction 41
3.4.3 Dielectric 48
3.4.4 Microwave 49
3.4.5 Infra-red 50
3.4.6 Laser 51

4 Bonding Mechanics Applied to Laser Welding **53**
4.1 Thermoplastic Bonding Physics 53
4.2 Thermoplastic Characteristics 54
4.2.1 Bonding Temperature 55
4.2.2 Material Properties 57
4.3 Thermodynamics and Heat Transfer 59

4.3.1 Steady State 61
4.3.2 Contact Resistance and Pressure 66
4.3.3 Temporal Effects 68
4.3.4 Advanced Modelling 72
4.4 Lessons from Laser Heating 74

5 Heating Thin Implants **77**
5.1 Properties 77
5.2 Feasibility 79
5.3 Experimental Performance 83
5.4 Welding Fixture 90
5.4.1 Thermal Resistance Issues 91
5.4.2 Cuvette Welding Success 93

6 Executive Summary **97**
6.1 Synopsis 97
6.1.1 Cuvette Assembly 97
6.1.2 Thermoplastic Welding Survey 98
6.1.3 Bonding Mechanics Applied to Welding 99
6.1.4 Heating Thin Implants 100

List of Figures

1-1 Daktari's first product, the Daktari CD4 16
1-2 Schematic of Daktari's cell chromatography technique (A and B) followed by electrochemical sensing (C) 21

2-1 Complete Dakrari CD4 cartridge assembly, with cuvette area highlighted 26
2-2 Conceptual exploded assembly that encloses the fluidic path and close up view of cuvette joining section 27
2-3 Issues of distortion of the side wall melting during the joining process 28
2-4 Rectangular dimensions of the cuvette 29

3-1 Hot gas welding 35
3-2 Schematic of the hot plate welding process 36
3-3 Image of commodity plastic bag impulse sealer 37
3-4 Schematic of ultrasonic welding and the efficiencies gained with the use of energy directors at the intended bond location 39
3-5 Resistive implant welding 41
3-6 A variety of schematics and methods of induction heating 43
3-7 Prototype induction welding setup to determine feasibility 44
3-8 In house testing of inductively heating of electrode material demonstrates some melting of the PMMA. Inductive heating solutions are also demonstrated in the literature 47
3-9 Everyday food items that utilize microwave susceptor heating 49
3-10 Initial concept testing of microwave heating of a conductive implant . 50
3-11 Through transmission laser welding 51

4-1 Phases of bonding. The molecular chains are free to move across the interface in reptation. Once the reptation time has elapsed, the chain has no memory of its original configuration 54

4-2 Summary of physical properties for common microfluidic thermoplastics 55

4-3 Specific volume versus temperature dependence in semi-crystalline compared to amorphous thermoplastics 56

4-4 Material map of thermal conductivity compared to expansion 58

4-5 Most thermoplastics have material properties that vary with instantaneous temperature and pressure, making it difficult to analyze during dynamic welding process 60

4-6 Equivalent thermal circuit for the cuvette 63

4-7 Relative thermal resistances experienced by each system side compared to that side's total modelled thermal resistance 65

4-8 Breakdown of thermal resistances on each side of the cuvette. Resistances pertaining to the lid side are exploded. In steady state, $\bar{H}$ results in a nearly symmetric HAZ for the laser model 66

4-9 Other laser considerations that affect the HAZ and actual image of heat affected zone 67

4-10 Effect of the residual gap on energy required for bond strength 68

4-11 Transient temperature distributions with gradients shown as a simplified semi-infinite solid for the constant surface heat flux boundary condition 69

4-12 Heat flux of the laser, q''_x, as a function of distance from the laser-transparent component top towards the weld interface at the absorptive component. Heat flux dependency on extinction coefficient, K, also illustrated 70

4-13 The effect of the non-dimensional Biot number in solids relating the spatial gradients of temperature in a solid relative to its surrounding 72

4-14 Temperature distribution across the external surfaces of the microfluidic system recorded with IR camera and compared to multi-physics simulations. DI water heated at the inlet with a resistive heater at a flow rate of $40\frac{mL}{min}$ 74

5-1 Implant cross section (not to scale). 78
5-2 Experimental implant initial tests and schematic 80
5-3 On left, current density versus current for the tested cross section with manufacturer maximum indicated. On right, energy generated versus current with the aforementioned current maximum configuration as well as $\dot{E}_{g,max}$ indicated 80
5-4 Thermal model of an implant generates energy ($\dot{E}_g$) symmetrically embedded between cuvette components and exposed to the ambient . 81
5-5 On left, predicted volumetric heat flux of the implant with manufacturer maximum indicated. On right, heat flux flowing normal to the bond interface, with rated maximum indicated. The curves are identically shaped with a difference in scales attributed to a factor of $\frac{1}{2}h$ . . 82
5-6 Preliminary desktop experimental setup with $15V$ $3A$ power supply, handheld thermocouple thermometer, and PMMA bonding jig 83
5-7 Initial implant trials prove the feasibility of heating with direct current 85
5-8 Data taken during initial testing provided insight into operational variables during implant bonding with a fixed electric potential provided by a power supply 86
5-9 Modifying the thermocouple placement results in a more realistic temperature reading of the PMMA bonding that occurs 87
5-10 Nuances in dealing with the conductive implants 88
5-11 Testing with the DAQ and constant current power supply provides further characterization of the welding temperature and power response and a correlation between temperature and resistance 89
5-12 Fixture design and implementation 90

5-13 It is apparent that the thermal resistance balance is an issue in the lack of welding 91
5-14 A comparison of the thermal resistances of the new versus original fixture in attempt to understand the inability for the new fixture to successfully weld 92
5-15 Backbone is now directly exposed to the ambient under the implant rather than through an insulator and the fixture 94
5-16 Implants aligned with the new fixture cutouts can bond two sides of the cuvette as testing progresses toward a complete cuvette seal . . . 95

List of Tables

3.1 Frequencies and methods used in electromagnetic bonding 40

Chapter 1

Introduction

This research focuses on development of manufacturing processes for Daktari Diagnostics's CD4 counter medical device. The ability to accurately measure CD4 levels with a low cost, portable, and easy to use product will benefit millions of HIV infected patients who cannot access expensive diagnostics. Significant innovation in microfluidic manufacturing methods are required for the Daktari CD4 product, specifically with regard to controlled manipulation and measurement of bio-fluids and assembling microfluidic systems to demanding tolerances at low cost.

1.1 Company Background

Daktari Diagnostics is a medical diagnostic device company located in Cambridge, Massachusetts. Daktari's mission is to create simple, accurate, and affordable products that address the most pressing challenges in global health. The Daktari team of engineers, scientists, physicians, and global health experts is uniquely dedicated to making high-performance products specifically designed for resource-poor markets. They are committed to delivering critical diagnostic test results to clinicians and patients across the globe. With the slogan, *today there is no place out of reach*, Daktari is developing a point-of-care (POC) CD4 level counter specifically designed for patients with HIV in resource-poor settings (Figure 1-1). [1]

1.2 A Global Health Need

1.2.1 HIV & AIDS

Since 1981, over 30 million people have died from AIDS. In 2010 alone, it is estimated that 1.8 million died from AIDS and 2.7 million have been infected by HIV. Today, there are more than 35 million people living with HIV and AIDS worldwide. This number is increasing according to UNAIDS' *2011 World AIDS Day Report.* [2]

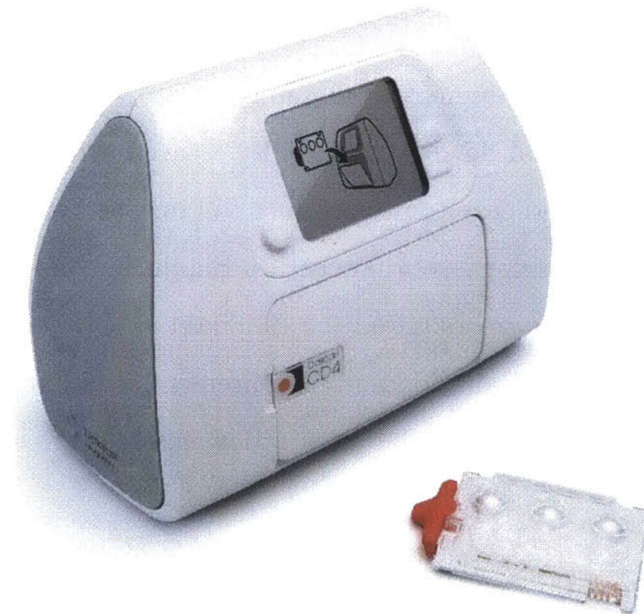

Figure 1-1: Daktari's first product, the Daktari CD4

Human Immunodeficiency Virus (HIV) is a virus that attacks the human body's immune system. Specifically, HIV affects CD4 cells (a type of white blood cell) that coordinate the immune system to fight disease by sending signals to activate the body's immune response once foreign bodies like viruses and bacteria have been detected. CD4 cells are attacked and impaired by HIV until the body's immune system reaches a point where it looses its ability to combat disease. This leads to an increased risk to opportunistic infections, a medical condition known as Acquired

Immune Deficiency Syndrome (AIDS). [3] Healthy, HIV-negative people typically have a CD4 counts of 600-1200 cells per mm^3. [4] A CD4 level of less than 200 cells per mm^3 indicates an AIDS diagnosis. [5] The measurement of CD4 is therefore useful to:

- Measure immune system strength of those infected with HIV
- Properly indicate when to start treatment to
    - prevent drug resistance caused by prematurely medicating
    - reduce the risk of patient drug-related side effects
- Monitor effectiveness of HIV treatment (every 3-6 months)

Flow cytometers, the modern standard equipment to perform CD4 diagnostic cell counts, are complex machines that cost between $30,000-150,000 and take up to 24 hours to provide results. While millions of people now have access to life-saving drugs, 70% of the worldwide HIV-infected population does not have access to necessary diagnostics, preventing them from receiving proper treatment. [6]

1.2.2 Point-of-Care Diagnostics

Across the industry, there is a tendency to relocate health care services away from centralized hospitals and directly to patient at the point of care. While this trend provides patients with options in countries with mature infrastructure, POC technologies may be the only viable way to treat many in resource-limited settings. The quality of healthcare facilities vary widely in developing countries and rural branches commonly have only basic equipment. In fact, electricity and running water cannot be guaranteed to be available. In addition to the scarcity of resources, healthcare workers may have little training to maintain complex equipment, with the shortage in many African countries as extreme as one qualified technician for every million people. [7] Therefore there is a need for diagnostics that feature reproducible and accurate results in a short time frame while still being low cost and require little user

training. The POC technologies must be rugged, portable, and consume little power in order to be operational in a variable environment for maximum efficacy on the health of users in resource-limited settings. [8]

1.3 LOC to POC

Lab-on-a-chip (LOC) technology has been applied to several of the four most common centralized hospital laboratory techniques: blood chemistries, immunoassays, nucleic-acid amplification tests, and, most relevant to CD4 counting, flow cytometry. Promising LOC medical diagnostic systems are being developed to obtain results from complex fluids with efficiency and speed without the need for an expert operator, attributes that will make POC applications possible for the most resource-limited settings [9]

1.3.1 Microfluidics

Most LOC systems utilize emerging *microfluidic* technology. The term *microfluidics* refers to the science and technology of systems that process or manipulate small ($< 10^{-6}$L) amounts of fluids and use channels with proportional dimensions of tens to hundreds of micrometers. [10] In microscale fluidic systems, surface tension, energy dissipation, and fluidic resistance significantly contribute to flow dynamics. In particular, the Reynolds number, which compares the effect of the fluid momentum to the effect of its viscosity, can become very low, resulting in a highly laminar flow system in which fluids do not regularly mix. [11]

1.3.2 Advantages

These small scale systems are advantageous for many reasons. Using small fluid volumes mean lower storage volume requirements, lower cost with reduced material usage, and less waste. Also, small channels allow for more rapid testing procedures including heating, mixing, and diffusion as necessary. Smaller size and lower energy

requirements allow for high parallel processing for increased throughput, all while permitting the use of disposable systems aimed to compete with the multi-million dollar laboratories of many hospitals. [12] The primary theoretical advantages of microfluidic systems are outlined as follows:

- Efficient use of reagents helps minimize costs
- Modular design allows flexibility
- Faster results (potential for real time analysis)
- Precise control over small fluid volumes
- Low cost of production

A wide array of microfluidic components such as micro pumps, valves, mixers, etc have been developed. A development that is analogous to the semiconductor industry, has led to highly integrated LOC systems now applicable to medically beneficial POC diagnostic devices. The core technology of Daktari is based on recent LOC microfluidic advancements.

1.3.3 Industry Note

Despite academic and commercial interest to create microfluidic medical diagnostic devices, few technologies have progressed beyond academic publication to become commercially available products. Micron scale features that permit precise control over solution manipulation conflict with the low cost mass manufacture constraints for resource-limited settings. Extremely small assemblies are more susceptible to physical anomalies that are otherwise ignored in macro applications. Tolerances must be scaled accordingly to the micro geometry and practitioners are confronted with uncharacterized phenomena that present new obstacles. Costs must be additionally balanced against market drivers, the people and governments that are purchasing the POC product. Daktari is at the forefront of developing product in this space, frequently innovating to solve new challenges.

1.4 Product Development

Daktari's first product will be Daktari CD4, a CD4 cell counting system designed to be portable and robust enough to be used in the most remote POC settings (Figure 1-1). The product's technology overcomes the two critical barriers, complex sample preparation and fragile, expensive optical sensors that restrict flow cyctometers from POC HIV testing. [1]

1.4.1 Cell Chromatography

Daktari's sample preparation technology, known as *microfluidic cell chromatography*, isolates cells and other particles in a microfluidic sensing chamber. It does not require pipetting, labels, or reagents, nor other complex manual steps typical of other blood tests. For Daktari CD4, the chromatography is accomplished by the binding of whole blood, including cells with CD4, to antibody manufactured into the channels in a process termed functionalization. Then, a specific shear force washes cells out of the chamber, save those with the CD4 protein. This is depicted in Figure 1-2, steps A and B. [13, 14]

1.4.2 Electrochemical Sensing

Daktari CD4 also takes advantage of a second innovation, *lysate impedance spectroscopy.* The system uses a simple sensor that counts the captured CD4 cells by measuring their internal contents electrically. The handheld instrument interprets the electrical signal, and reports the CD4 count within minutes [1] More specifically, the CD4 cells membranes are ruptured (lysed) within a high-impedance solution (Figure 1-2, step C). The ionic contents of the cell are released into the solution and the change in impedance is measured. This difference compared to the baseline is proportional to the CD4 count and used for the simple diagnostic reading. The method proves to be inexpensive and robust, as it it is unencumbered by the lenses, cameras, filters or complex optics of other diagnostic tests like flow cytometry. [6, 15]

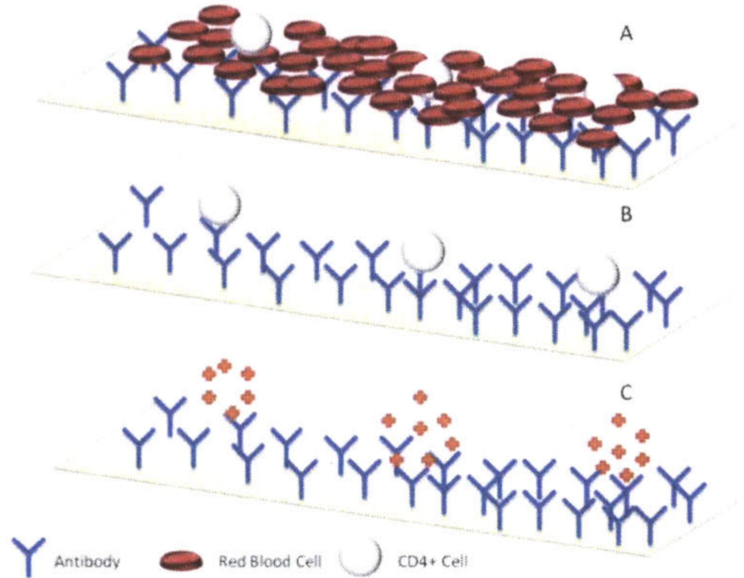

Figure 1-2: Schematic of Daktari's cell chromatography technique (A and B) followed by electrochemical sensing (C)

1.4.3 Pressing Challenges

For Daktari, the specific most pressing challenges include:

- Controlling fluid flow at microscale levels
- Fabrication of microscale devices on mass producible materials
- Using and storing sensitive solutions in off-the-shelf materials
- Low-cost fabrication and integration of electrical components

Manufacturing precise micro channel pathways and fluidic manipulation mechanisms is key to accurate microfluidic control. Precise component assembly is critical for diagnostic results. Therefore, there is a need for the development of more capable processes that meet stringent microfluidic product functional requirements as the development and performance evaluation of the Daktari CD4 continues .

1.5 The MEng Capstone Project

This document serves as partial fulfilment of the graduation requirements for the Masters of Engineering in Manufacturing program at the Massachusetts Institute of Technology. Through the Department of Mechanical Engineering's Laboratory for Manufacturing Productivity (LMP), the work is co-advised by Professor David Hardt and Brian Anthony, director of the MEng program. The author conducted the research and laboratory experiments documented in this thesis at Daktari Diagnostics, advised on site by Robert Etheridge, Vice President of Operations. Four students actively worked at Daktari, each focusing on a unique manufacturing challenge of Daktari's HIV diagnostic. The author of this thesis, Benjamin Judge, developed a method of heating a proprietary metal pattern for the immediate use of sealing clear microfluidic channels. Nikhil Jain focused on reducing variability in high-throughput electrode production, with a primary emphasis on the system-critical impedance measurements. [16] Tejas Inamdar and Aabed Saber conducted work on characterizing the effect of bonding process parameters during assembly and the resultant effect on reagents. [17,18]

1.6 Thesis Overview

This body of work is organized in the following manner: Chapter 1 outlines the company, market, and key technology of Daktari's CD4 product. The key functional requirements pertaining to the product's most critical feature, the cuvette, is described in Chapter 2. Chapter 3 surveys methods for bonding thermoplastics in the context of considering an approach that will meet the requirements of the cuvette. Assembly and bonding processes are analyzed in Chapter 4. Building on laser welding insights, a method of heating thin implants to the bonding temperature of the assembly is explored in Chapter 5. Finally, Chapter 6 summarizes conclusions drawn from analysis and testing in an effort to provide recommendations for cuvette bonding and future work in the space.

1.7 Focus of Thesis

Recently, Daktari has begun to utilize a flexible, robust, and low cost electrode production process in order to accomplish reliable electrochemical sensing. Building upon Daktari's unique conductive pattern deposition method, this thesis focuses on novel applications of the technology, specifically for localized resistive heating of the patterns as conductive implants. Resistive heating was attempted in response to Daktari's need for of assembling their CD4 product. Methods developed have applications across the industry, as the functional requirements of different microfluidic platforms could be met with inexpensive electrically conductive components. While the resistive heating application is applied to the present need for precise bonding of microfluidic thermoplastic systems, the anticipated need for heating biochemical assays in future LOC/POC products, and other unanticipated applications in which the aforementioned conductive material is used in such a way that current flow or electric potential produces resistive heat losses to be characterized and/or sensed.

Chapter 2

Cuvette Assembly

The *cuvette* is the working name for Daktari's most difficult to manufacture micro feature. Generally, a cuvette is a small tube designed to hold samples for spectroscopic experiments. In Daktari's product, it refers to the location of the microfluidic channel where cell chromatography and electrochemical sensing of CD4 cells occurs (shown in the context of the larger self-contained cartridge in Figure 2-1). The cuvette is composed of a three sided feature molded into a 2mm thick backbone and a 250μm thick cover lid, known as the electrode foil. [19] The ideal cuvette would be optically clear and without imperfections that prevent a clean reading from the lysate impedance spectroscopy process. On the contrary, current assembly processes result in sensing that suffers from noise and produces a product that is opaque.

2.1 Material Selection

The micron geometry scale size of LOC systems like Daktari's lends itself to standard silicon processing technique of the semiconductor industry. In fact, microfluidic research in academia traditionally utilizes soft lithography via casting of a clear and inert silicon-based organic polymer, Polydimethylsiloxane (PDMS). [20] Constructing microchannels with PDMS work relies on conformal contact in assembly. Employing at least one soft, elastic, and conformal surface not only provides a degree of forgiveness for imperfections of the surface, but also permits sharp corners and dimensions

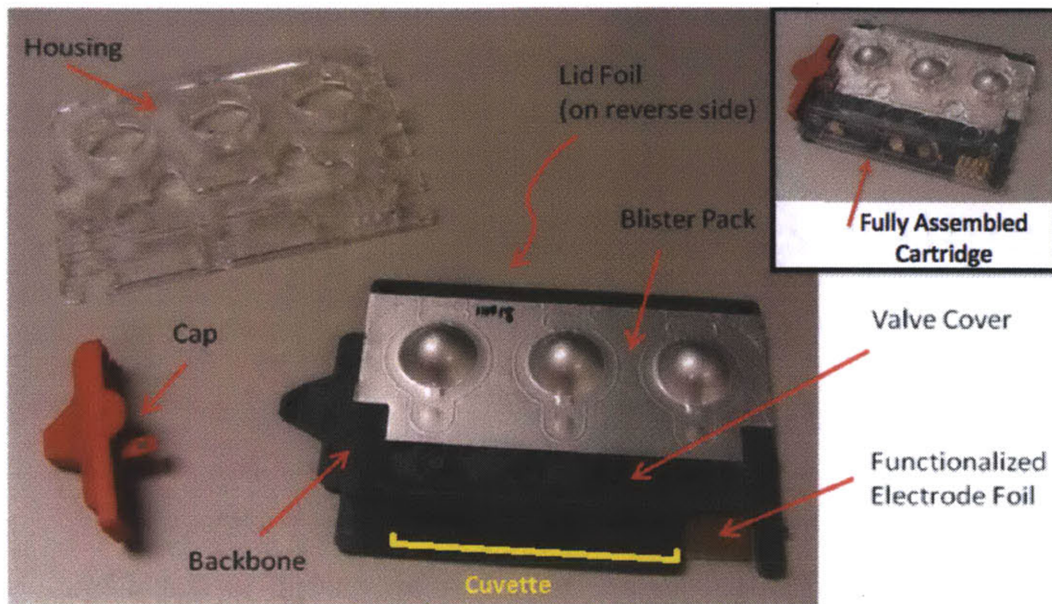

Figure 2-1: Complete Dakrari CD4 cartridge assembly, with cuvette area highlighted

below the micro scale that meet Daktari's geometric requirements. Figure ?? is an example of a precisely fabricated PDMS cuvette prototype in an academic lab [14]. However, since the Daktari system is being designed for mass manufacture, thermoplastic polymer materials are a better material selection, even though they are not substantially soft or conformable [21].

Thermoplastics polymers have significantly lower raw material manufacturing costs compared with more traditional microfluidic materials (e.g. silicon and glass). Small scale fabrication and prototyping can be carried out using methods such as direct micro milling, hot embossing, and laser ablation. However, the standard mass production method of injection molding polymer systems is preferred to realize the greatest economy. [21] Daktari has partnered with the premier micro injection molding expert to produce its complete CD4 cartridge assembly according to the *Functional Requirements* 2.4. PMMA (acrylic) is easy to injection mold and is qualified for FDA compliant devices. This research will focus on methods and applications dealing with a PMMA cuvette. More specific detail of working with thermoplastics like PMMA is found in Chapter 4.

2.2 Cuvette Assembly

Regardless of material or method of manufacture, almost all microfluidic platforms include an open microchannel that requires an assembly step that caps and encloses the fluidic paths (Fig. 2-2(a)). The Daktari cartridge with cuvette feature is too complicated and costly to design as a single part, a typical situation of microchannels designed for mass production.

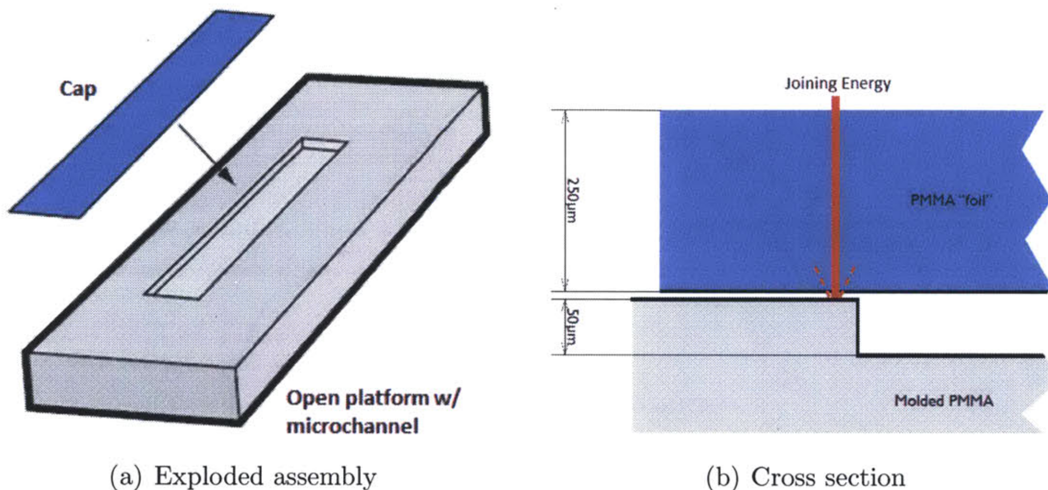

(a) Exploded assembly

(b) Cross section

Figure 2-2: Conceptual exploded assembly that encloses the fluidic path and close up view of cuvette joining section

2.3 Assembly Issues

Despite being common application in the microfluidic industry, bonding of the cuvette proves problematic. The process is serial, presents difficulty in clear part bonding, is very sensitive to air gaps that disrupt intended thermal loads, and the process is difficult to get in manufacturing control to meet geometric design requirements. Even after best efforts at optimization, bon-uniformity of the cuvette sidewall exists at the cuvette edge relative to design specification (Figures 2-3(a)). This results in the failure to meet the geometric functional requirements, and it has been observed to actively

introduce noise in the impedance reading. The measurement noise is hypothesized to be a result of trapping particles in the laser-deformed gaps as the assay is run.

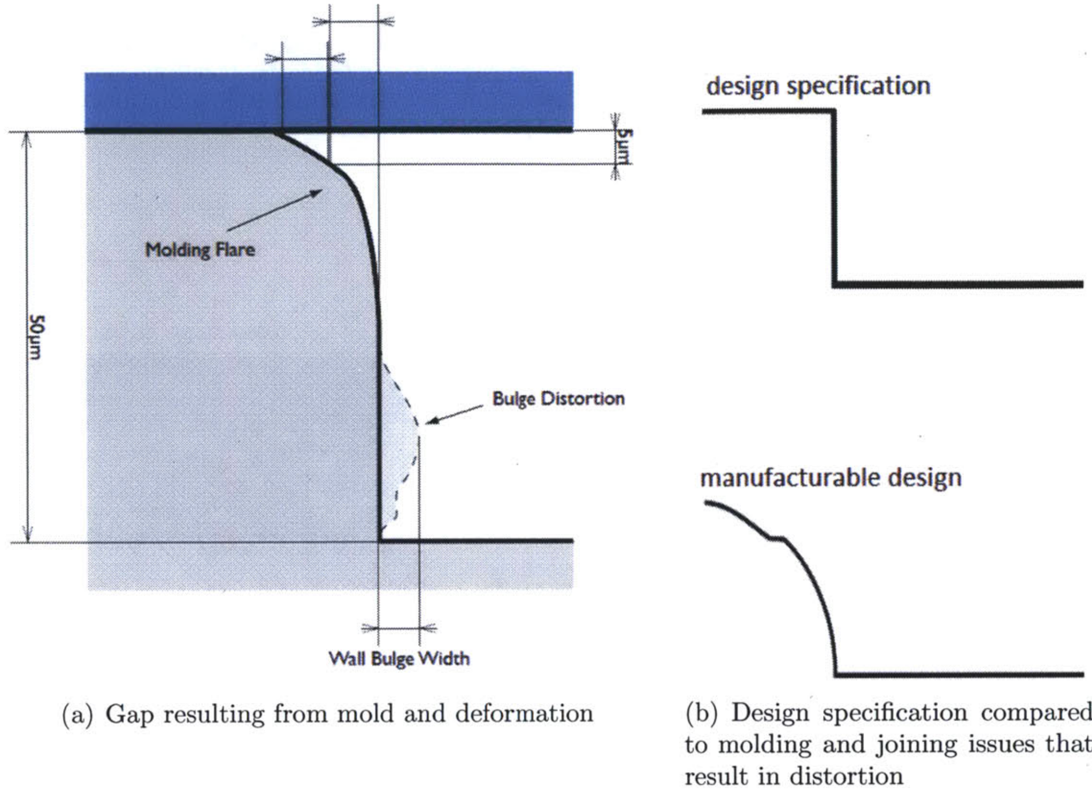

(a) Gap resulting from mold and deformation

(b) Design specification compared to molding and joining issues that result in distortion

Figure 2-3: Issues of distortion of the side wall melting during the joining process

2.4 Functional Requirements

Whether using the laser or an alternative technique, any cuvette assembly process used must meet a set of predetermined design guidelines. The designer needs to be cognisant of many operational requirements in order to select viable manufacturing techniques for a mass produced diagnostic cartridge. Based on Daktari's initial technology development, the most recent *System Product Requirements*, outlines the following set of functional requirements for the cuvette:

2.4.1 Geometric Dimensioning and Tolerancing

The cartridge shall have a microfluidic feature with appropriate dimensions with walls as vertical as possible and with corners as square as possible to perform an assay.

Rectangular Dimensions

$50\mu m \pm 1\%$ x $4mm \pm 10\%$ x $50mm \pm 10\%$

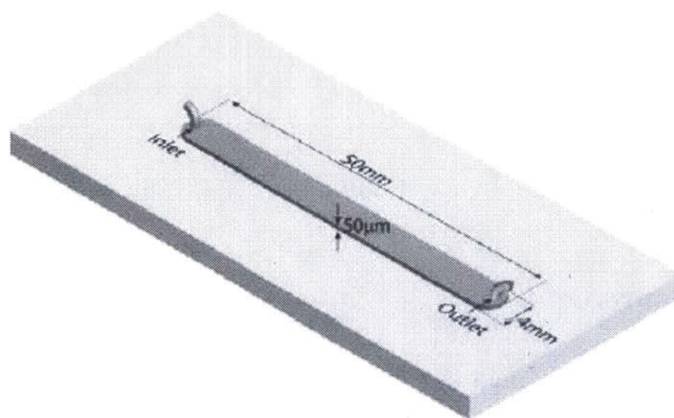

Figure 2-4: Rectangular dimensions of the cuvette

Squareness

Wall verticality and corner radii are yet to be determined, but are based on sensitivity to fluid dynamics and contaminant size. This area of work has been identified as critical with respect to trapping contaminants.

2.4.2 Fluid Dynamics

Flow Rate

The cartridge shall be capable of pumping the fluids through the cuvette at a requisite flow rate and sustain a test pressurization.

Mixing

The fluidic channels should be designed to minimize the mixing of reagents during flow through them, and to minimize the effects of contamination blood particulates.

2.4.3 System Performance

In general, the system must function as outlined in the aforementioned core technology (Section 1.4.1) when accepting samples of whole blood.

Functionalization

The cuvette shall have one large surface (for instance the backbone *floor* or electrode *ceiling*) treated with functionalization chemistry (e.g. antibodies).

Impedance Measurement

Similarly, the cuvette shall have one large surface on which sensing electrodes have been formed, capable of measuring the impedance curve when cells are lysed in an appropriate length of time with minimal signal noise.

Other

Normal exposure to chemicals to which the product is intended or expected to contact shall not impact system performance. These may include sweat, alcohol, and commonly used disinfectants. The product should be reasonably resistant to water but shall not be required to be submersible. The product shall be designed so that users are exposed only to non-hazardous materials based on the appropriate regulatory requirements for this product.

Equivalence

New process cannot change precision, accuracy, dynamics, or specificity by affecting antibody, electrode function, channel geometry.

2.4.4 Design for Manufacturing

The system should be designed with appropriate considerations for manufacturing and assembly. As the product is developed, considerations must be made for materials, processes, supply chains, and labor requirements that meet market needs and product placement goals.

Cost of Goods Sold

The cost of goods sold (COGS) for the cartridge is essential to the product being marketable in resource limited settings. Therefore the cartridge plus packaging and shipping costs should be minimized.

2.4.5 Design for R&D

As the product is being developed, certain characteristics designed into the product make it easier for internal testing and iteration.

Fluid Ports

All fluid ports for blisters, vias, and sample entry should be capable of connection to an external syringe for development stage testing.

Optical Clarity

To observe all of product's fluidic flow during tests in real time, the cuvette must be optically clear. This is a requirement for effective in-house assay development.

In-House Assembly

Fast, iterative design is essential for efficient product development. Reducing the number of dependencies on external partners and enabling in-house assembly of the microfluidic cuvette increases the ability to experiment quickly to prove concepts that progress the design.

2.5 LOC Industry Context

The assembly of microfluidic channels such Daktari's cuvette is an area in want of innovative solutions. Many functional requirements of Daktari's product, especially the cuvette, apply across the LOC industry. According to academic literature and conversations with practitioners, the deformation of microchannels during assembly is a significant obstacle. As the industry develops LOC devices for mass production with increasing function and demanding requirements, more precise and flexible thermoplastic micro-scale assembly techniques becomes more valuable. [9,22–30] This thesis will explore alternative methods of microchannel assembly. The implemented method is studied and generalized to apply to proposed alternatives in Chapter 4. In addition to assembly, the demonstrated method of heating resistive implants (Chapter 5) may have applications in other functions of microfluidic systems throughout the industry.

Chapter 3

Thermoplastic Welding Survey

Several methods for permanently sealing thermoplastic microfluidic structures exist. Methods are chosen for cost, short bonding times, good joint mechanical properties, and high levels of consistency. Mechanical joining via mechanical fasteners, clinch joints, snap fit, fasteners, or other types of preloaded contact may meet product functional requirements. [31, 32] However, a mechanical seal at the microfluidic interface may not exhibit the potential integrity that can be realized with a complete polymer *bond* at the molecular level. Leakage in preloaded embodiments is a concern, particularly if the part is warped or experiences runout due to manufacturing. The product must also be robust to use scenarios where ageing, environmental effects, or human handling may disturb the mechanical fasteners. Instead, the following section reviews the bonding methods that create complete hermetic joints in thermoplastic polymers with respect to the assembly of the cuvette.

3.1 Bonding Classification

According to Tsao's survey on microfluidic bonding, bonding techniques may be classified as either indirect or direct. [28] Indirect bonding utilizes an additional layer such as an adhesive to seal the substrates and encapsulate microchannels. Direct bonding methods mate the substrates without any additional materials. The differences are distinguished by direct bonding producing homogeneous sidewalls in the

microchannels that have no affect on chemical, optical, and mechanical properties over time. In PMMA, up to 80% strength of the virgin material can be realized in direct polymer bonding. [33] Since Daktari's product requires homogeneity of the microchannel, adhesives are not considered a design option. Only direct bonding methods are subsequently considered in the survey of this chapter, often described as polymer *welding*. The aforementioned direct and indirect classification will henceforth be described as *homogeneous* welding to differentiate it from direct and indirect application of welding energy to the intended bond interface described in Chapter 4.

3.1.1 Solvent

The addition of a solvent is technically an indirect method in that another material is added to the interface of the bond area. The solvent penetrates the thermoplastic surface causing swelling and plasticisation such that the polymer chains may diffuse. [31] Special care must be taken to ensure all of the solvent is ventilated from the end product, and consideration must be made with respect to emission control, flammability, crazing, and surface preparation. [34]

3.2 Welding with an External Heat Source

In general, thermoplastics have low coefficients of thermal conductivity compared to other materials like metals (see section 4.2.2). Using an external source of heat can create a steep thermal gradient normal to the bond surface (Figure 4-13(a)). Ideally this heat will soften or melt the bond area only locally. Adding heat energy in this way can be very flexible method of welding and require only minimal initial investment for a capable process. However, using external heat sources to weld may be slower, susceptible to flash or deformation if indirectly heating the bond interface, and have higher operating costs due to continuous resistive heating compared to other methods. [28, 31] Welding with an external heat source has been employed in several different welding techniques.

3.2.1 Hot Gas

Similar to the oxygas welding of metals, hot gas welding utilizes a consumable filler rod that is melted at the bond interface via a directed stream of hot gasses. Gas welding is typically a manual method depends on the skill of the operator. It does have the advantage of portability to a work site. [31, 35]. It is not possible for an operator to create a bead at the dimensions required in this application. Alternative applications include aiming the hot gas stream at the substrate directly and plastics susceptible to oxidation, inert argon or nitrogen can be used. Gases are an inefficient method of imparting heat energy compared to methods that follow. No vendors were discovered that could meet the functional requirements of Daktari's product.

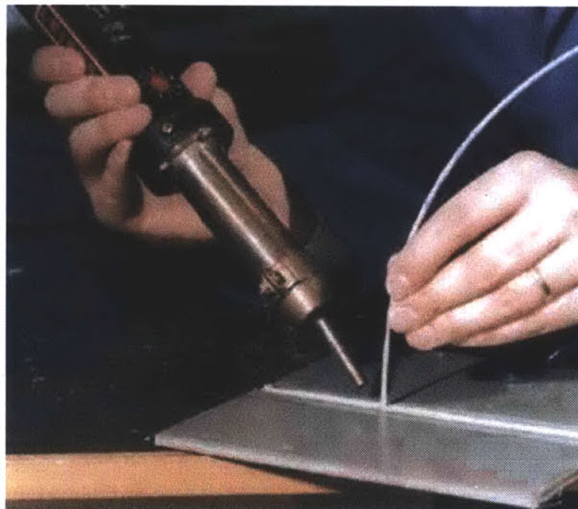

Figure 3-1: Hot gas welding

3.2.2 Hot Plate

Hot plate welding is probably the simplest technique for thermoplastics and typically has the lowest equipment cost. The parts to be welded are held in fixtures which press against a heated tool (plate, iron, etc). As shown in Figure 3-2, the heated tool melts and the thermoplastic surfaces are displaced against the tool until they are softened some distance away from it. The parts are then removed from the heated tool and

clamped together. As they cool, bonding occurs, usually with high weld integrity. Process parameters include plate temperature, pressure, time, and material. [34] The literature describes other microfluidic applications of thermal bonding. [36–38]

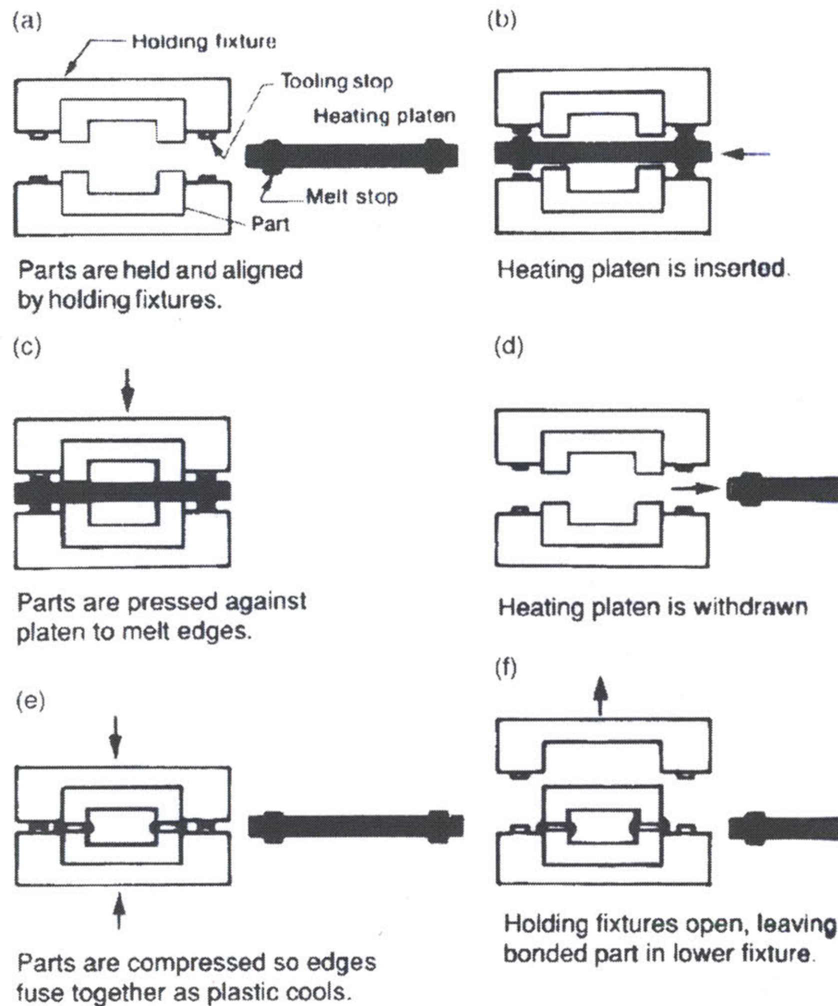

Figure 3-2: Schematic of the hot plate welding process

3.2.3 Hot Bar and Impulse

A variation of hot plate welding utilizes resistive bar elements to melt from the outside through the part and therefore typically is used for thin films ($< 0.5mm$). This method is used extensively in the packaging industry to seal plastic bags and can take

advantage of multi-layer substrates to tune the melted zones (Fig 3-3). In another embodiment, a very small wire is heated with an impulse of electricity. The small mass of the wire cools rapidly. While the part is under pressure, bonding with in a well controlled temperature curve can be realized. [39] An outside vendor was contracted for testing Daktari's application. They were unable to create a hermetic bond at the cuvette interface without deformation. Test results for moving the seal location outboard and relying on a mechanical preload at the interface should be feasible based on laser and cover foil bonding, but test results have not been conveyed at the time of writing.

Figure 3-3: Image of commodity plastic bag impulse sealer

3.3 Welding via Mechanical Movement

Rather than using an external source of heat, efficiencies can be realized when polymers have heating energy directed specifically at the interface to be bonded. When two surfaces are brought into contact and rubbed together under pressure, friction causes a temperature increase and heat flux. The rate of energy transferred to the interface is related to the speed of mechanical movement. Methods of bonding under the category of mechanical movement can be either linear or rotary in nature and occur at macro and molecular scales. They tend to be quick and inexpensive but have

limitations in size and shape as some require specific symmetry or special geometric features. Since parts are physically moving to generate heat, alignment proves an issue, as does noise generated in the workplace. [31]

3.3.1 Spin

The simplest embodiments of spin welding can utilize a drill or lathe to force one thermoplastic feature rotating into another. Purpose built machines are often used for greater control. Rotational speed, friction, pressure, displacement, and duration each effect the end weld. [34] Since spin welding is usually limited to axially symmetric shapes, there is limited use for Daktari's specific application.

3.3.2 Vibration

For thermoplastic pieces with linear joints such as car bumpers, vibration welding is utilized. The welders typically run at power main frequencies and the work piece is fixed to a bed of springs that resonates at 110 or 220 Hz. The springs self centers the part to some degree, though final alignment can prove difficult when as part ceases moving and solidifies. While it could be applied to microfluidics, designers tend to only choose this method if ultrasonic welding is not a possibility. [34]

3.3.3 Ultrasonic

Ultrasonic welders use high frequency sound energy to soften or melt the thermoplastic. Parts held under pressure and subjected to vibrations between $20 - 40kHz$, resulting in a very fast weld ($< 1s$) for automated mass production. A carefully designed piezoelectric transducer converts electrical to mechanical energy. A horn is used to amplify that energy, and a customized sonotrode transmits the vibrations to the workpiece. The bond location on the thermoplastic part must also include an *energy director* feature to concentrate energy to create the initial melt zone, shown in Figure 3-4(a). Intermolecular and boundary friction softens this zone and as the damping factor increases, the reaction accelerates causing a greater proportion of the

energy to translated into heat to flow directly at the bond region. Design considerations include minimizing the distance that the waves travel to the joint and careful sonotrode design to meet power and control limitations. [40] Ultrasonic machinery is thus limited to bonding only a small area at once.

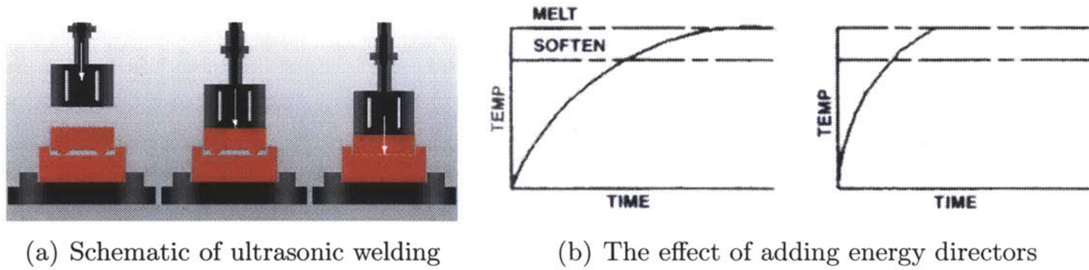

(a) Schematic of ultrasonic welding (b) The effect of adding energy directors

Figure 3-4: Schematic of ultrasonic welding and the efficiencies gained with the use of energy directors at the intended bond location

Academic research has demonstrated modified machines capable of bonding microfluidic scale features. [41–46] However, working with multiple leading vendors of ultrasonic bonding (including Branson™ and Hermann™ Ultrasonics), it was determined that the best feature size attained was $10\mu m$, and only with the significant modification of the design to include energy directors. The decision was made to not pursue development of ultrasonic methods since microfluidic welding scales are industrially unproven, capital equipment is expensive, proof of concept testing would not be accomplished in house, and the physics of ultrasonics are extremely difficult to characterize as energy is transferred through many different mediums. It remains a viable option for future in-depth study.

3.4 Welding with Electromagnetism

The final grouping of thermoplastic welding techniques directly employs electric or magnetic fields. Table 3.4 depicts the range of methods that utilize electromagnetism for homogeneous bonding, listed in increasing order of frequency. [31] It is important

to consider whether the material is an electric conductor or dielectric as their response to an electromagnetic field is an important design consideration. Methods can be non-contact, precise, rapid (reducing degradation and heat affected zone), and easily automatable. Initial equipment cost tends to be the highest and implants to focus energy can add extra cost, but direct coupling can realize long term operational efficiencies. [34]

Spectrum	f(Hz)	Welding Type	Applicator
DC-AC	10^0	Resistive implant	High current connectors
HF	10^6	Induction/hysteresis	Work coil
VHF	10^7	Dielectric	High voltage capacitor
Microwave	10^9	Susceptive implant	Resonant applicator
Infrared	10^{11}	Infrared	Focused infrared lamp
Infrared	10^{12+}	Laser	Mirrors, lenses, fiber optics

Table 3.1: Frequencies and methods used in electromagnetic bonding

3.4.1 Resistive Implant

Resistive implant welding is a simple and fast technique which can be applied to almost any thermoplastic. It involves trapping an electrically conductive insert between the two parts to be joined, followed by resistively heating the insert by passing a high electric current through it. The inserts are frequently made of metal wire, braid, or mesh to conduct direct current (DC) or low frequency alternating current (AC). As the implant heats due to resistive losses, the surrounding thermoplastic softens, to be welded once put under pressure and cooled. Recycling and bio-compatibility may be an issue, but implants are being utilized more frequently in advanced composites to be heating restively or inductively (see next section). [34] Both resistive implant heating via the application of current directly and inductively are the focus of the research of this work, and demonstrated using an adaptation of Daktari's electrode production technique in Figure 3-5(a). Please see Section 3.4.2 and Chapter 5 onward

for a more complete analysis of these methods.

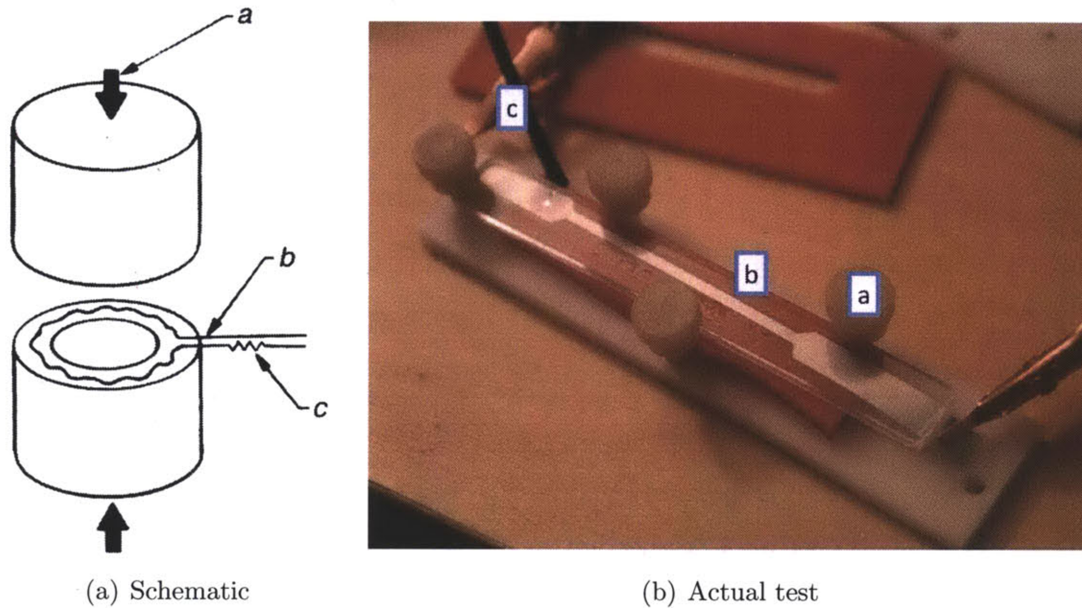

(a) Schematic

(b) Actual test

Figure 3-5: Resistive implant welding. A heated material is placed between the two thermoplastics where **a** is pressure, **b** is high resistance wire, and **c** is wire heat control

3.4.2 Induction

Induction techniques strictly describes welding where heating is generated by an inductive magnetic field. Otherwise, it is quite similar to the above mentioned resistive methods in that a conductive implant is generally required to be heated at the weld line. A work coil connected to a high frequency power supply is placed in close proximity to the implant at the joint. In induction, this implant is called a *susceptor*. A dynamic magnetic field generated from the coil is coupled to the susceptor, inducing electric currents that resistively heat the conducting material, softening the surrounding thermoplastic parts for welding. The susceptor coupled by the heating coil is analogous to a short-circuited secondary coil of a transformer. Via the *Joule* effect, high *eddy currents* are induced within the work piece and heat accord-

ing to Equation 5.9. Figures 3-6(a) and 3-6(b) depict general induction heating of a metal. [47]

Induction can be a very fast manufacturing technique in thermoplastic applications with a conductive implant, as in the assembly of container bottle caps (Figures 3-6(c) and 3-6(d)), hermetic aseptic food packages, grills on loudspeakers, and advanced composites. Published examples of inductive joining techniques are listed in patent literature for aerospace and even carpentry. [48–52] Relevant operational parameters include the coil resonant frequency, incident time, coupling distance, power, clamping pressure, susceptor design and complementary work coil design, and material properties (including geometry, resistivity, and permeability in addition to factors listed in Section 4.2.2). Other characteristics of induction welding are that it is a mature process for macro parts, has high throughput, precise control, low operating costs, reopenability, and nondestructive x-ray joint verification. Disadvantages are similar to resistive in the added cost associated with additional material, assembly, recycling contamination. There is typically a higher development cost to achieve the ideal coupling. Users must be equipped to handle appropriate magnetic field levels. [34] Inductive heating is one of two predominant techniques that achieves non contact welding by focusing energy for heating directly at the joint area, the other being laser methods described in Section 3.4.6 and Chapter 4.

Feasibility

Attempts at inductively heating components made with Daktari's electrode production process were carried out to discover its feasibility when applied to cuvette assembly. Instead of purchasing an expensive production heating unit, an inexpensive inductive stovetop unit was modified and a do-it-yourself (DIY) resonant circuit was created for experimentation. [53, 54] The DIY coil resonating at $150kHz$ quickly heated size 10 galvanized steel machine screws past water vaporization temperature. Household kitchen foil noticeably interacted with magnetic field forces and was heated to the point of incandescence.

The cooktop nominally resonated at $24kHz$ (load dependant) and has a manu-

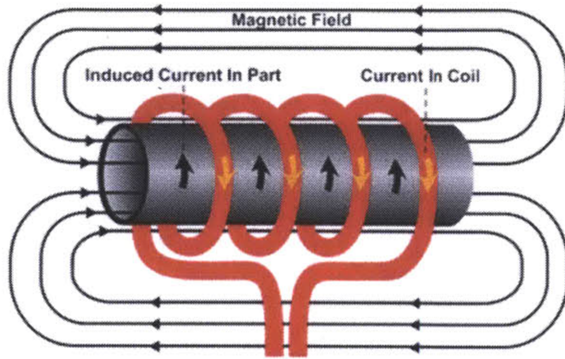

(a) General induction method

(b) Inductively heating a turbine blade

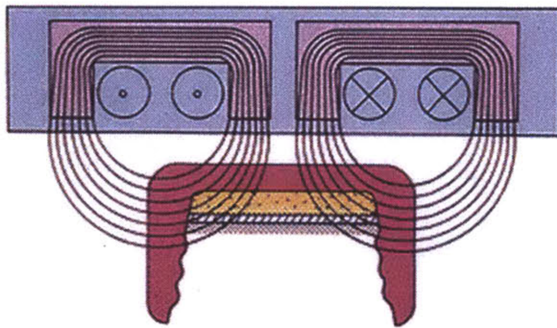

(c) Schematic of bottle sealing

(d) Bottle sealing manufacturing line

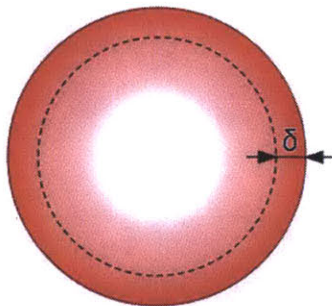

(e) For AC, most electrical current flows between the surface and skin depth, δ, which depends on the frequency of the current and the electrical and magnetic properties of the conductor

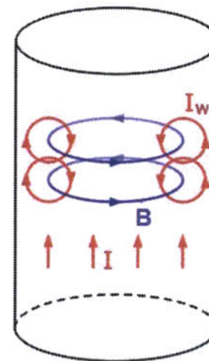

(f) The faster the magnetic field (B) changes, the more current flow is cancelled out in the center of the conductor, reinforcing the skin effect

Figure 3-6: A variety of schematics and methods of induction heating

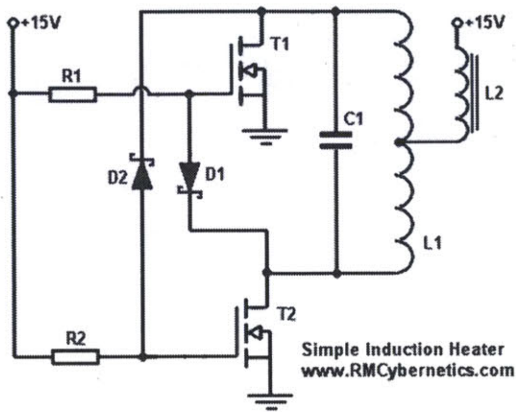

(a) Complete heater resonant circuit diagram

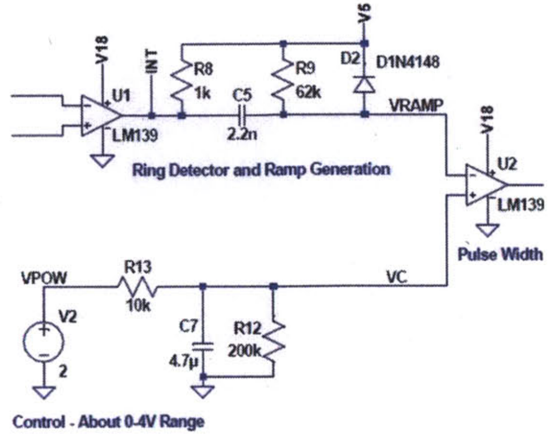

(b) Cooktop controller diagram for pot sensor

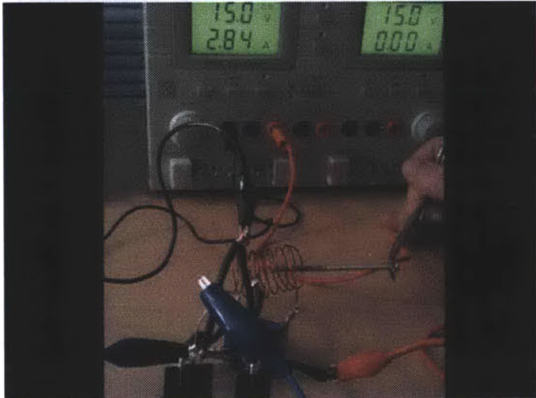

(c) DIY induction coil heating size 10 bolt

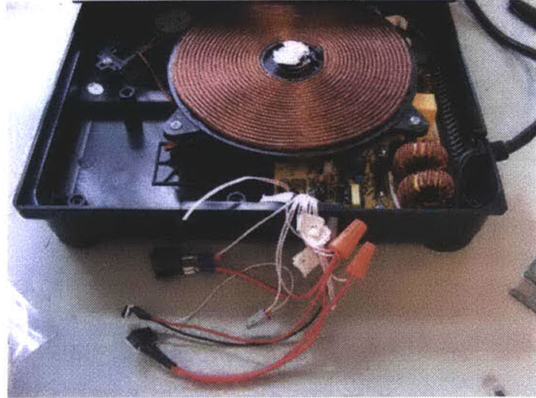

(d) Modified induction cooktop

(e) Non conductive induction clamp and test samples

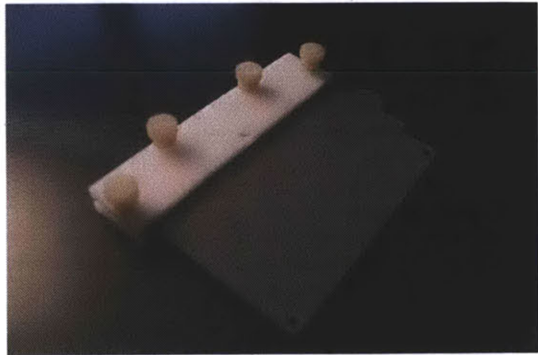

(f) Clamp will accept complete production backbone

Figure 3-7: Prototype induction welding setup to determine feasibility

facturer rated power of $1.8kW$. An optimized iteration of the DIY coil resonated at $250kHz$, powered by a supply capable of $45W$ at the MOSFET rated operating voltage of $15V$. Both instances had some heating response in the electrode material to the point that some melting of PMMA occurred, demonstrated in Figures 3-8(a) to 3-8(d). However, when the non-conductive test clamp was fabricated to accept production samples for inductive heating, shown in Figure 3-7(e), it did not result in any detectable temperature response.

It is clear the aforementioned embodiments have enough power to melt the very small mass of electrode material. It is therefore assumed that the material to coil coupling must be refined. The work coil must be properly designed to inductively heat the thin susceptors. The perfectly coupled case of actual physical contact at $0Hz$ direct current would be the limiting case, with the testing in Chapter 5 demonstrating low wattage requirements for melting plastics by resistive heating with conductive susceptors (aka implants). Upon further review of induction literature, it is determined that skin effects illustrated in Figure 3-6(e) take an important role in not only high frequency work coil design with respect to it over heating, but also in efficient coupling to the susceptor. The system must be tuned to the appropriate operational *penetration depth* (akin to the conductor skin depth phenomenon but with a reversed logic; the work coil magnetic field frequency change determines the depth to which eddy currents penetrate). Additionally, internal friction of magnetic materials, hysteresis heating, becomes relevant if conductors are ferrous. [55–58]

Knauf has focused his doctoral work inductively heating thin susceptors in the context of microfluidic bonding (Figure 3-8(e)). Usable heating was only demonstrated at frequencies and powers levels much higher than listed in this work's induction experiments, indicating difficulty in efficient coupling. Regardless, experimental insights were documented such as that microfluidic induction bonding times were short, hotspots frequently occurred, power pulsing was useful to prevent burning, diamagnetic metals could be heated, and finally, that at certain penetration depths the measured temperature was independent of frequency. At high frequencies and power levels, sub-micron susceptors located at the minimum coupling distance from

the work coil achieved heating rates of $30\frac{^oC}{s}$. Knauf also articulated the difficulty of processing complex susceptors within microfluidic assemblies, but took advantage of existing induction heating equipment provided by the German firm, Hűttinger Elektronik [30, 59–62]

Induction heating consultants were then contacted to determine if any sort of temperature response could be detected with samples made from the Daktari electrode production process. Inductive bottle sealing expert Enercon Industries Corporation stated they were unable to heat materials that thin, nor were their salespeople familiar with induction frequency dependence. Ambrell® Precision Induction Heating articulated that they were not able to heat the provided samples at $380kHz$ on a $10kW$ heater. Similarly, Superior Induction Company attempted $300KHz$ at $7kW$ without success, citing there was not enough mass of metal for the induction heater to target, but believed much higher frequencies could do the job.

It is surmised that the traditionally macro scale heating solutions that the aforementioned vendors typically supply are not designed to couple to microfluidic susceptors. In particular, the coil design is much more sensitive for the thin electrode material system at hand. Like high performance transformers, the magnetic field produced by a particular work coil configuration is imperative for efficient coupling to the susceptor. While the samples provided were the same thickness in the direction normal to the PMMA lid material, the susceptor provided to the vendors was a thinner trace created to be representative of the actual required cuvette bond line. It was intentionally a more ambitious design since preliminary feasibility of the material was accomplished at Daktari with the DIY and cooktop work coils. It was presumed that vendors would be able to heat components with appropriate coupling for a high volume microfluidic product in order to sell their capital equipment and support. No vendors were discovered that successfully heated the Daktari material.

While feasible, inductive heating methods will be an area for future development. Like microscale ultrasonic methods described in Section 3.3.3, substantial research, testing, and design must occur before inductive cuvette bonding is a realistic manufacturing process. This includes the initial simplification of the susceptor for R&D to

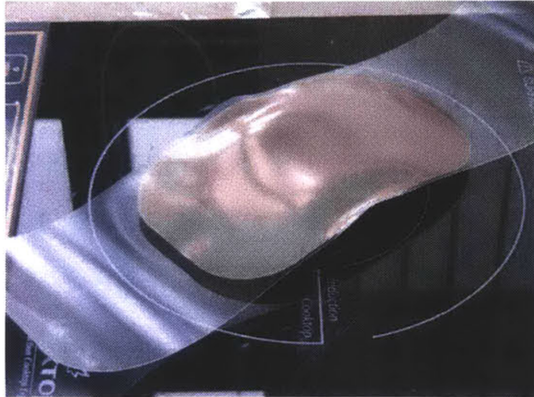

(a) Large section of electrode material melts PMMA via current eddies along major axis

(b) Higher frequency DIY resonant coil utilizes Litz wire to run cooler

(c) Coil quickly heats kitchen foil to glowing temperatures

(d) Pancake coil melts PMMA with a large section of thin susceptor

(e) Knauf's closed loop, $1mm$ thick, etched $7.5\mu m$ thick Ni susceptor following channels at an offset of $1mm$ come close to a complete seal

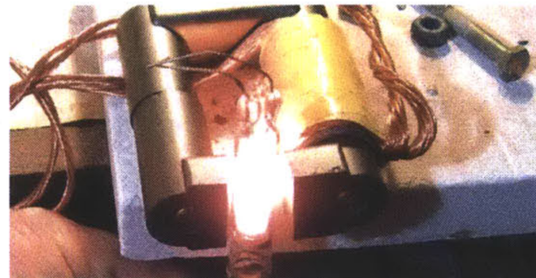

(f) Demonstration of DIY flux concentrator heating from Fluxeon

Figure 3-8: In house testing of inductively heating of electrode material demonstrates some melting of the PMMA. Inductive heating solutions are also demonstrated in the literature and in industry

reduce the number of variables, modeling all of the related rates with multi-physics software, and investigating advanced magnetic engineering methods like flux concentrators to aid in solving coupling challenges (Figure 3-8(f)). [63] Instead, the general mechanics of plastic bonding and development of the related resistive heating in conductive implants occurs in Chapters 4 and 5, respectively. It is recognized that with the completion of this foundation of characterization from DC to AC resistive heating followed by inductive coupling, a scalable non-contact mass assembly process for Daktari's CD4 product becomes realistic for thin implant heating such as cuvette welding.

Electro-Magnetic Assembly

Electro-Magnetic Assembly (EMA) welding is a proprietary method from Emabond Solutions™. They harness the phenomenon of hysteresis loss in a ferromagnetic material implant when it is subjected to a high frequency work coil. Emabond tunes the induction field strength to melt an iron based particulate filler for a thermoplastic joint. Since hysteresis loss is frequency dependent, the power supply must source AC between $2 - 10GHz$. As the material is heated and crosses the *Curie point* and become paramagnetic, a novel heat control method occurs as hysteresis heating ceases until the part cools below Curie temperature. Emabond claims that unlike heating exclusively by eddy currents produced in normal induction, EMA is able to produce long linear welds. Their products come in standard sizes for a limited number of thermoplastics. [64] The use of this method is currently under review by Emabond at the time of writing.

3.4.3 Dielectric

At very high electromagnetic frequencies, the molecules in a material will vibrate. Dielectric welding produces a field at 27.12 MHz that makes the part's molecules oscillate and heat for a weld. No prior work was discovered referring to the efficacy for microfluidic applications, but Daktari's requirements are currently under review

with vendors of dielectric bonding equipment. [65]

3.4.4 Microwave

An analogous alternative to inductive methods is bombarding the work piece with microwave radiation. Like induction, most thermoplastics do not experience a temperature rise when exposed to microwaves and thus a microwave susceptible implant is required at the joint line to couple the energy. The phenomenon is exploited in home microwave ovens to heat food. Aluminum particulate susceptors in many snack packages are tuned to the oven's $2.4GHz$ operating frequency (Figure 3.4.4). [66, 67]

(a) Hot Pockets®

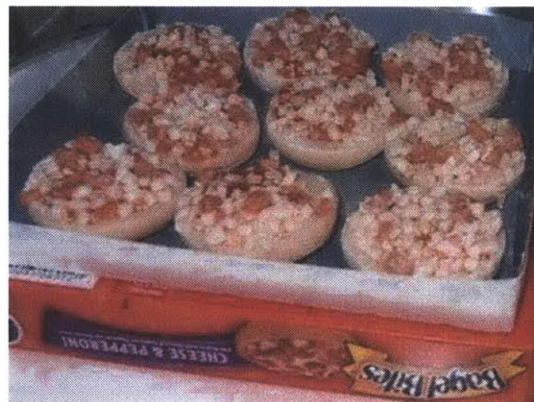

(b) Bagel Bites®

Figure 3-9: Everyday food items that utilize microwave susceptor heating to super heat foods beyond water boiling temperature in order to crisp

Academic research outlines the potential for microfluidic microwave bonding. Waveguides can create zones of high microwave concentration in free space through which parts could be conveyed and coupled to a microwave susceptor (antenna). [68, 69] Initial testing shows that using an implant in a microwave oven is difficult to control. Runaway heating and vaporization of the implant ensues due to high voltage potentials in the metal. Testing that resulted in destroyed samples and a proposed schematic of heating phenomena are depicted in Figure 3.4.4. Work in the microwave

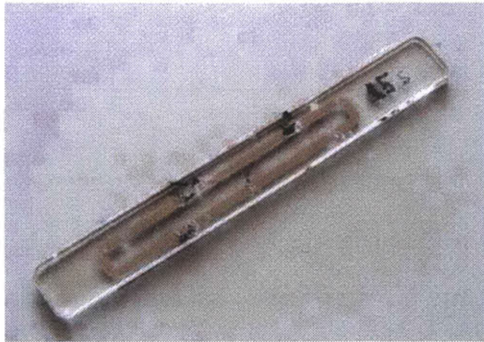

(a) Home microwave experiment with implant

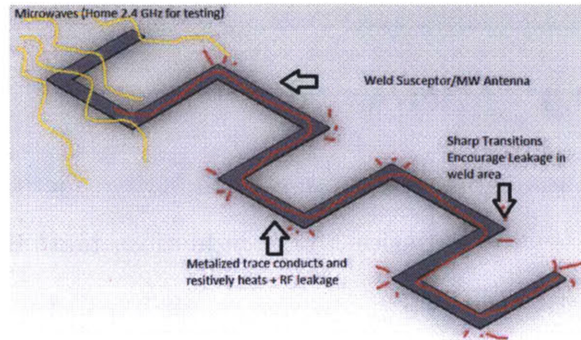

(b) Preliminary schematic of assumed microwave heating phenomenon, though more research in high frequency phenomenon is required

Figure 3-10: Initial concept testing of microwave heating of a conductive implant

domain will not be pursued to solve Daktari's need for assembly techniques. However, lessons learned in the high frequency resistive heating of an implant are useful in characterizing the frequency range required to couple with the implant as it applies to lower frequency methods of electromagnetic bonding.

3.4.5 Infra-red

Infra-red radiation welding is similar to hot plate methods (section 3.2.2), but no physical contact is required as it heat is radiated toward the components. Infra-red welding is typically faster and contamination is reduced compared to using a hot plate, but its ability to create fine welds is limited since the energy is produced with lamps and transferred through the part to the weld interface, rather than focused or directly coupled. Energy absorption is also color and material dependent; the thermoplastic must absorb infra-red wavelengths. It is sometimes used in conjunction with other methods to preheat the work piece, as in hybrid laser welding. [33] Efforts at infra-red bonding are outlined in the MIT thesis *The Development of an Innovative Bonding Method for Microfluidic Applications.* [70]

3.4.6 Laser

Lasers have only been used industrially for polymer bonding since the 1990s. Lasers allow a novel method of bonding known as *through transmission infra-red welding*, depicted in Figure 3-11(a). In its most basic embodiment, the upper layer is transmissive to the laser wavelength and the lower absorptive. The laser heats the absorptive material and expands, increasing weld pressure. At the focus of the beam the power is at a maximum and a melt zone initiates. Once sufficient molten material is created via melting and increasing pressure, a weld is formed. [33]

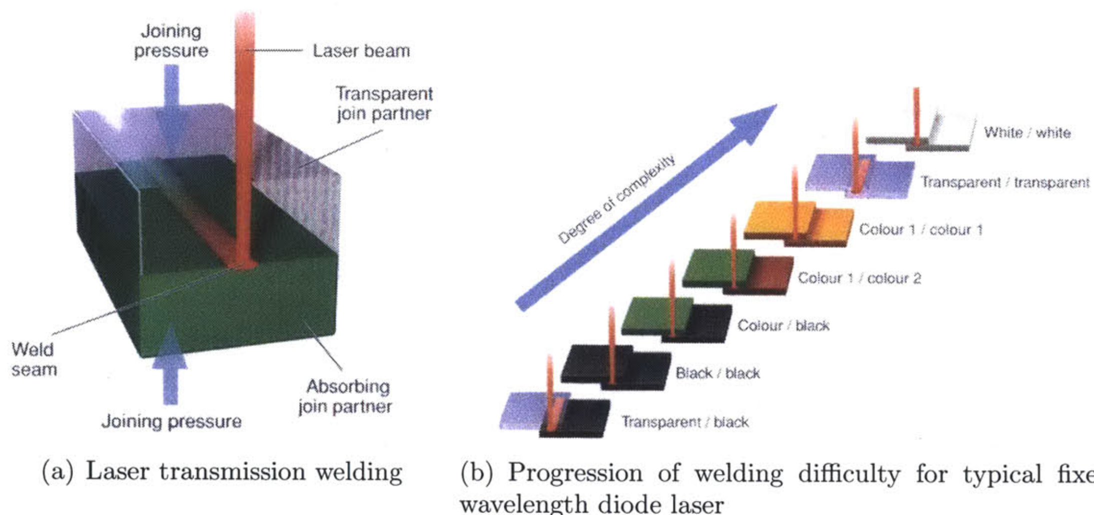

(a) Laser transmission welding

(b) Progression of welding difficulty for typical fixed wavelength diode laser

Figure 3-11: Schematic and degree of complexity in the color combination of transparent and absorptive laser join partners in through transmission laser welding

The advantages of this welding method are many, and include being non contact, low pressure, sub-surface, precise, having a small heat affected zone (HAZ), reduced mold cost (no directors), no flash, no additional materials, hermetic seals, flexible pattern, immediate handling, the ability to weld very small parts, and efficiency ($< 100W$ for diode units with $1\mu m$ laser wavelength). Disadvantages include high capital costs, being limited to bonds between clear and opaque materials, and inflexibility to hight variations (beam focusing) or air gaps. [34] More advanced tunable or $2\mu m$

lasers are required for heating of transparent components directly, but care must be taken since the $2\mu m$ wavelength would also heat the normally transmissive part. Tuning to the polymer absorption maxima is required. For the typical diode lasers, the most difficult colors to weld are shown in Figure 3-11(b)). Otherwise the addition of special absorptive additives such as Clearweld® must be added to the interface, making the joint non-homogeneous. Nonetheless, welding by laser is the method of choice for applications requiring high levels of precision or those that cannot handle particulates. The absence of heat and vibration permit the joining of sub assemblies with sensitive components, which is becoming increasingly popular in everything from automotive to medical applications, and particularly in commercial LOC products. The commercial microfluidic use of laser bonding is analyzed in greater detail in Chapter 4.

Chapter 4

Bonding Mechanics Applied to Laser Welding

In this chapter we explore the theory associated with bonding thermoplastics and the relevant thermodynamic and heat transfer mechanisms in welding with a laser. Lessons learned will be applied to new implant based techniques in Chapter 5.

4.1 Thermoplastic Bonding Physics

The requisite bonding forces between mating surfaces are generally due to molecular entanglement or charge interactions. Entanglement happens through the mechanical interlocking of polymer chains across a plurality of surfaces. Typically, a modification of the interface energy is necessary. [31] The additional energy increases the free volume in the region of the weld. As the mating parts are brought into intimate contact, polymer chain diffusion through the free volume creates a joint with integrity on par with the original material in a process known as *reptation*, shown in Figure 4-1. [70].

Efficient mixing and interaction of polymer chains is a function of high interfacial compatibility that depends on internal bond structures. Therefore, bonding at high temperature can greatly enhance polymer entanglement and interaction at the interface, especially for bonding two surfaces of the same material. Using weld-

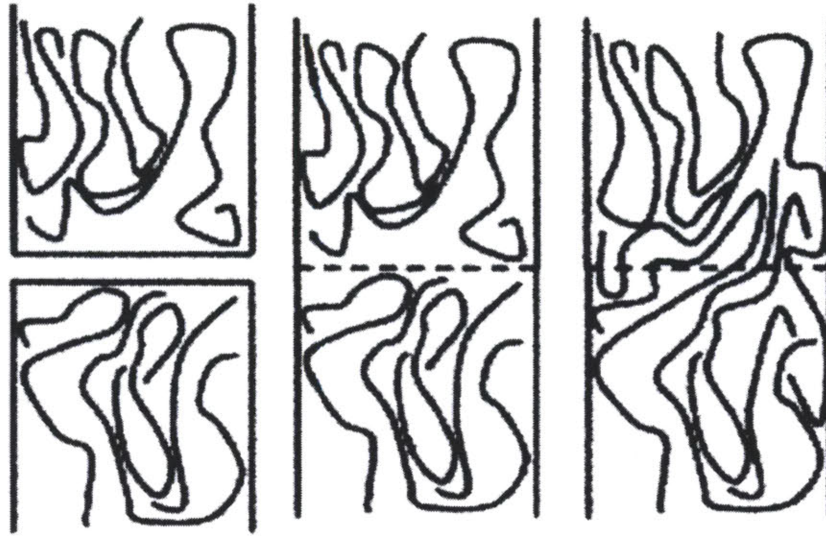

Figure 4-1: Phases of bonding. The molecular chains are free to move across the interface in reptation. Once the reptation time has elapsed, the chain has no memory of its original configuration

ing to enclose microfluidic channels without deformation is particularly demanding, with minimal heating and melting usually desired. High clamping pressure or surface wettability is therefore preferred to promote more intimate contact between mating surfaces during bonding applications at lower temperatures. However, most thermoplastic polymers used in mass produced products have low-energy, hydrophobic surfaces. The resultant poor wettability precludes the use of many low temperature techniques. [28] Thus, a careful characterization of thermoplastic properties with respect to thermal methods are required for effective welding.

4.2 Thermoplastic Characteristics

Ideal thermoplastics for medical diagnostic production have engineerable material properties. These include high chemical resistance (to hydrolysis, acetone, or acids), minimal water absorption, and optical clarity as outlined in Section 2.4. [26,71] Popular thermoplastic polymers that meet common requirements for mass manufacture are

cyclic olefin copolymer (COC), polycarbonate (PC), and, Daktari's selection, polymethylmethacrylate (PMMA). Figure 4-2 lists some of the relevant parameters of common thermoplastics. [28]

Polymer	Acronym	T_g (°C)	T_m (°C)	CTE (10^{-6}°C^{-1})	Water absorption (%)	Solvent resistance	Acid/base resistance	Optical transmissivity	
								Visible	UV[a]
Cyclic olefin (co)polymer	COC/COP	70–155	190–320	60–80	0.01	Excellent	Good	Excellent	Excellent
Polymethylmethacrylate	PMMA	100–122	250–260	70–150	0.3–0.6	Good	Good	Excellent	Good
Polycarbonate	PC	145–148	260–270	60–70	0.12–0.34	Good	Good	Excellent	Poor
Polystyrene	PS	92–100	240–260	10–150	0.02–0.15	Poor	Good	Excellent	Poor
Polypropylene	PP	−20	160	18–185	0.10	Good	Good	Good	Fair
Polyetheretherketone	PEEK	147–158	340–350	47–54	0.1–0.5	Excellent	Good	Poor	Poor
Polyethylene terephthalate	PET	69–78	248–260	48–78	0.1–0.3	Excellent	Excellent	Good	Good
Polyethylene	PE	−30	120–130	180–230	0.01	Excellent	Excellent	Fair	Fair
Polyvinylidene chloride	PVDC	0	76	190	0.10	Good	Good	Good	Poor
Polyvinyl chloride	PVC	80	180–210	50	0.04–0.4	Good	Excellent	Good	Poor
Polysulfone	PSU	170–187	180–190	55–60	0.3–0.4	Fair	Good	Fair	Poor

T_m melting temperature, *CTE* coefficient of thermal expansion

[a] high UV transmissivity often requires the selection of special polymer grades, e.g. without stabilizers or other additives

Figure 4-2: Summary of physical properties for common microfluidic thermoplastics

Thermoplastics are a class of synthetic polymers (plastics) that soften above a characteristic temperature but still remain dimensionally stable over a wide range of working stresses. The softening (and subsequent complete melting) is due to the long-range motion of the polymer molecular backbone. Thermoplastics differ from *thermoset* polymers by their ability to be reshaped after being fully or partially melted and subsequently return to its original chemo-physical state upon cooling. This thermoplastic phenomenon is exploited in joining. [31] Thermoplastics suffering only minor degradation when repeatedly heated rather than experiencing a chemical change, as opposed to thermosets that becoming irreversibly cross-linked.

4.2.1 Bonding Temperature

A further distinction exists within thermoplastics to be either *amorphous* or *semi-crystalline*. The difference is illustrated by the temperature-volume dependency in Figure 4-3(b) compared to Figure 4-3(a). [31,34] *Semi-crystalline* thermoplastics ex-

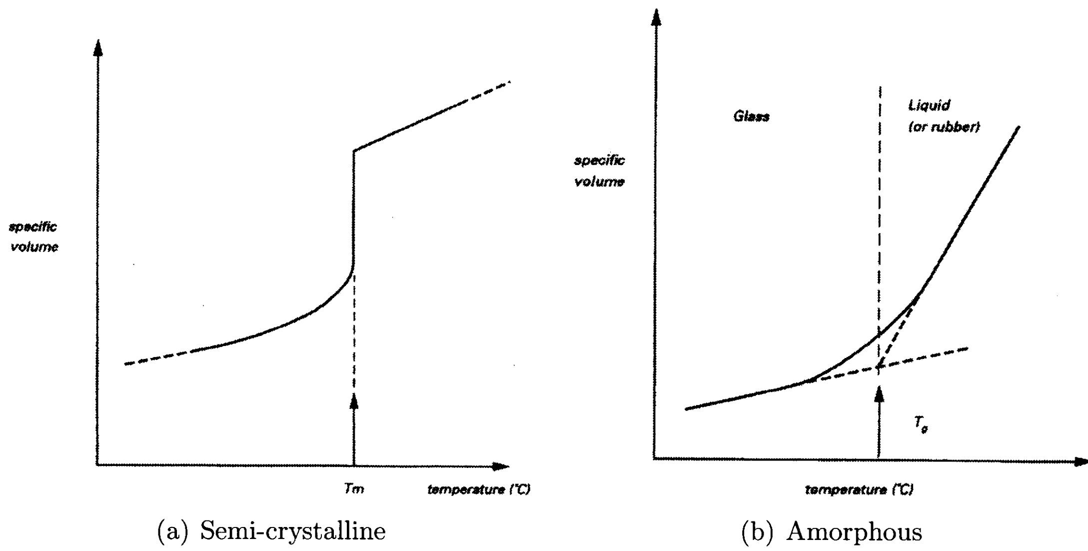

(a) Semi-crystalline

(b) Amorphous

Figure 4-3: Specific volume versus temperature dependence in semi-crystalline compared to amorphous thermoplastics

hibit a regularly repeating lattice structure between small amorphous areas with a very specific melt temperature (T_m). However, *amorphous* thermoplastics have molecule chains existing as randomly dispersed coils that cause a *glassy transition temperature* range (T_g). [33] Therefore, there exists a temperature window for amorphous thermoplastics within which it can be bonded (listed in Figure 4-2). [28] Thus,

- Heating above T_g for amorphous thermoplastics
- Heating above T_m for crystalline thermoplastics
- Using a solvent to reduce T_g to ambient temperature
- Changing the surface molecular charge or chemistry

each induce polymer flow (reptation) at the intended bond interface and can create a homogeneous weld when components are brought into contact. While crystallinity properties can sometimes be advantageously engineered, (amorphous PMMA can

have a 50% smaller laser weld bead than some semi-crystallines), bonding temperature, T_{bond}, is dependant on a combination of other temperature dependant material properties and instantaneous system parameters. [33] Therefore there is not a rigidly defined T_{bond}, nor cuvette failure temperature, T_{fail} within T_g for Daktari's cuvette welding application.

4.2.2 Material Properties

In addition to the temperature required for welding, design for PMMA welding is dependant on a number of other material properties. Thermoplastics tend to be much more compliant (lower Young's Modulus) with lower strength than other materials. Combined, these parameters can determine a plastic's resiliency under loading conditions, though this limit is usually not approached in microfluidic applications.

PMMA's molecular level configuration determines the amount of energy required to change its temperature. This intrinsic material property is scaled with the solid's density to determine the engineering property of volumetric heat capacity, c_p, in units of $\frac{J}{m^3K}$. c_p is dependent on temperature and is comparatively small with respect to the spectrum of materials (analogous to plastic's relatively low density). *Thermal conductivity*, k, describes energy transport through the material and is also a temperature dependent property. k is in units of $\frac{W}{mK}$ and is low in plastics compared to other materials. The ratio of k to c_p is termed a substance's *thermal diffusivity*

$$\alpha = \frac{k}{c_p} \tag{4.1}$$

and has units of $\frac{m^2}{s}$. Plastics have low thermal diffusivity and thus respond slowly in time to temperature as heat energy conducts slowly through its thermal bulk. PMMA will take a comparatively long time to respond to its environment and reach thermal equilibrium compared to metals.

Figure 4-2 lists the *coefficient of thermal expansion*, CTE, of microfluidic thermoplastics in units of $\frac{10^{-6}m}{mK}$. The CTE tends to be high for plastics. For a given increase in temperature, PMMA will volumetrically expand more than many non-

thermoplastics. Along with α, CTE is an essential thermal property to consider in welding of thermoplastics, and is logarithmically mapped versus k in Figure 4-4. [72]

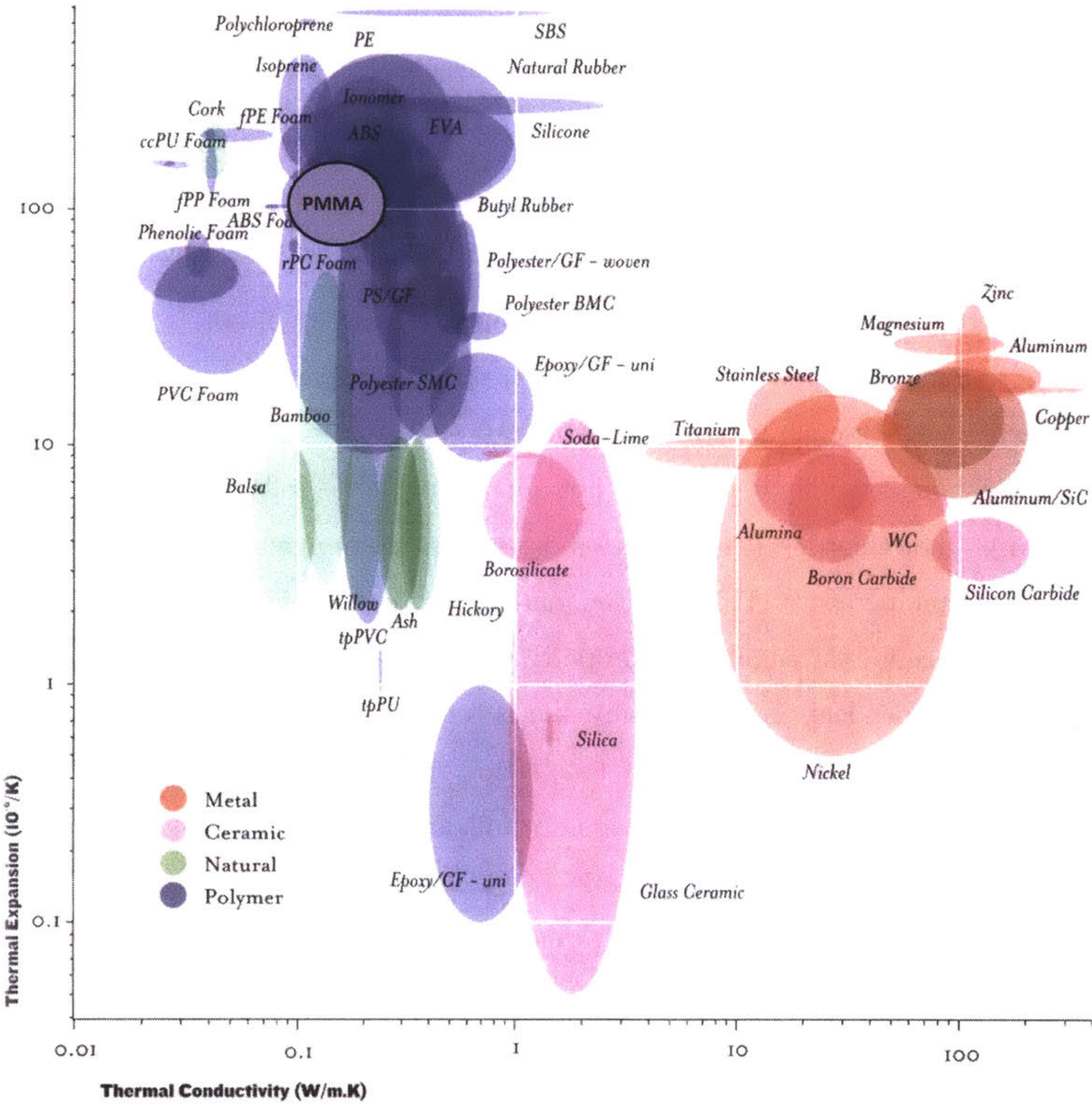

Figure 4-4: Material map of thermal conductivity compared to expansion

While metals tend to have high conductivities with low expansion, polymers have k values that are 1000 times less and CTE around 10 times greater. It is therefore critical to match CTE when adjacent materials experience high temperatures since internal stresses result from the different expansion rates. This is particularly relevant

to plastic parts interacting with metal welding fixtures or heated platens. Selecting an appropriate k is valuable in the design of heat sinking or insulating properties of the welding system. Each of the aforementioned parameters of the thermoplastic PMMA will come into play when analyzing cuvette welding. It should be noted that listed values are only valid instantaneously for standard temperature and pressure. Almost all thermoplastic material properties vary with a change in temperature and pressure (Figure 4-5(a)

4.3 Thermodynamics and Heat Transfer

A more general thermal model of applying energy to plastic can be obtained through thermodynamic and heat transfer theory. *Thermodynamics* concerns the *equilibrium* or *steady* states of matter and necessarily precludes the existence of a temperature gradient in time. *Heat transfer* quantifies the rate energy change occurs during thermal non-equilibrium, rather than just the final amount of energy required to pass from one equilibrium state of the thermoplastic system to another. Heat transfer analysis provides an intuition of critical parameters to consider while exploring bonding methods and oberving results. The following derivations of Section 4.3 are based on Incropera and DeWitt's *Fundamentals of Heat and Mass Transfer.* [73]

According to conservation of energy on a time basis, the rate at which thermal and mechanical energy enters a control volume ($\dot{E}_{in}$), plus the rate at which thermal energy is generated within the control volume ($\dot{E}_{gen}$), minus the rate at which thermal and mechanical energy leaves the control volume ($\dot{E}_{out}$) must equal the rate of increase of energy stored within the control volume($\dot{E}_{stored}$). A general form of the energy conservation requirement may be expressed on a rate basis as

$$\dot{E}_{in} + \dot{E}_{gen} - \dot{E}_{out} = \frac{dE_{stored}}{dt} \equiv \dot{E}_{stored} \tag{4.2}$$

Inflow and outflow terms are typically control surface phenomenon of the thermoplastic such as conduction, convection, and/or radiation and are proportional to surface area, matter advection, or work interactions. The energy generation term,

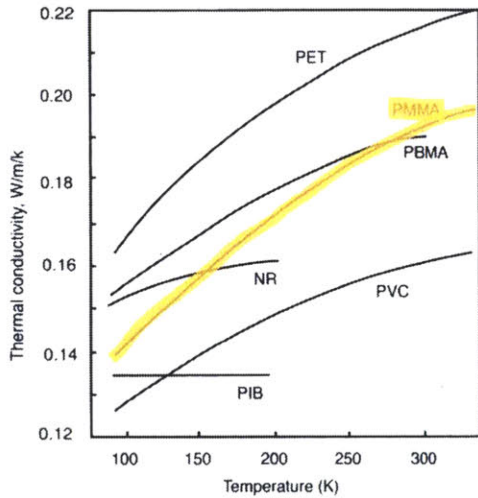

(a) Thermal conductivity versus temperature

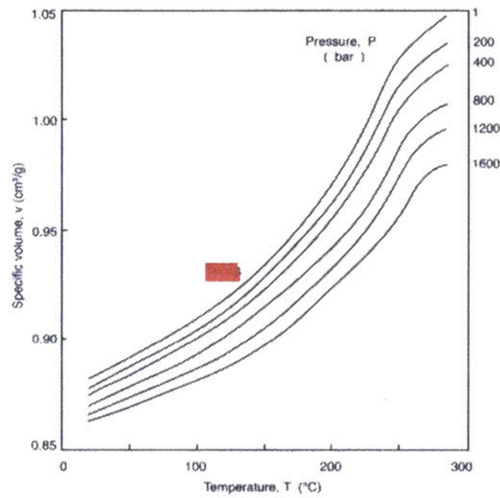

(b) Examplar pressure, volume, and temperature diagram for polymide 66

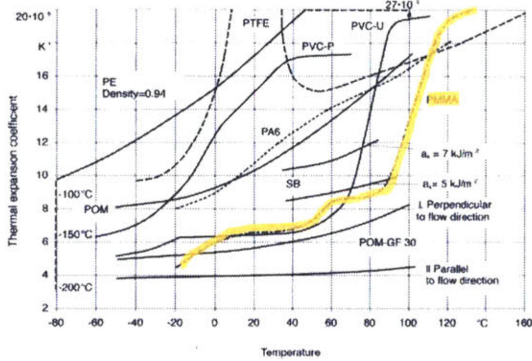

(c) CTE versus temperature

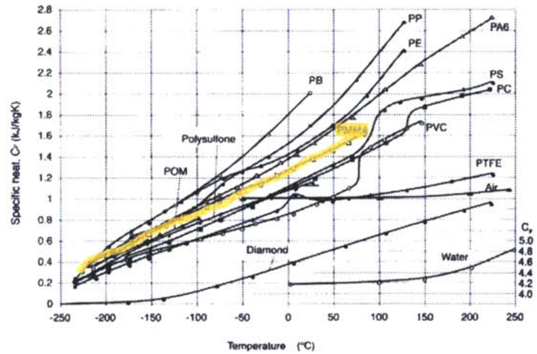

(d) specific heat versus temperature

Figure 4-5: Most thermoplastics have material properties that vary with instantaneous temperature and pressure, making it difficult to analyze during dynamic welding process

$\dot{E}_{gen}$, is associated with a conversion of from some other energy form (chemical, electrical, electromagnetic, or nuclear) to thermal energy and is a volumetric phenomenon of the actual bonding process. For instance, the added energy due to laser radiation or electrical energy being converted heating due to absorption or resistance, respectively, corresponds to the rate at which energy is generated (released) within the volume of interest. For the cuvette, the region of interest is the intended hermetic bond interface.

Fourier's law is the rate equation to describe the amount of heat energy being transferred per unit time for any solid that experiences heat conduction, like a thermoplastic. For a simplified one dimensional plane having a spatial temperature distribution $T(x)$, the rate expression is expressed as

$$q''_x = -k\frac{dT}{dx} \tag{4.3}$$

The *heat flux*, q''_x, is the heat transfer *rate* in the x direction per unit area perpendicular to the direction of transfer. q''_x is in units of $\frac{W}{m^2}$ and is proportional to the to the spatial temperature gradient, $\frac{dT}{dx}$, in x direction. The minus sign is a consequence of the fact that heat is transferred in the direction of decreasing temperature.

Using both Equations 4.2 and 4.3, the *Heat Diffusion Equation* is defined in one dimension as a function of volumetric heat generation ($\dot{q}$), the material's conductivity, and volumetric specific heat capacity

$$\frac{\partial}{\partial x}\left(k\frac{\partial T}{\partial x}\right) + \dot{q} = c_p\frac{\partial T}{\partial t} \tag{4.4}$$

4.3.1 Steady State

Using the heat equation 4.4, we can make a simplification of the cuvette thermal system by assuming heat transfer is one dimensional, the system is in steady state, no heat is generated, heat flux is constant, and thermal conductivity is constant in order to utilize thermal resistance principles to model thermodynamics. The assumption for thermal equilibrium and consequently the steady state simplification implies such

that enough time has passed that temporal gradients have ceased ($\frac{dT}{dt} = 0$). Thus, the appropriate form of the idealized heat equation is

$$\frac{d}{dx}\left(k\frac{dT}{dx}\right) = 0 \tag{4.5}$$

Integrating 4.5 twice and using Fourier's Law 4.3, we have the required heat flux for the bonding process at thermal equilibrium:

$$q'' = \frac{\Delta T}{\sum R''_t} \tag{4.6}$$

where ΔT is the overall temperature difference bounding $\sum R''_t$, the summation of the *thermal resistances* of a composite wall made of any number of series or parallel R''_t due to layers of different materials, plus contact resistance parameters ($R''_{contact}$) between intermediate layers (in units of $\frac{m^2K}{W}$). Heat is conducted through the cuvette and fixture, so their thermal resistances are of the form

$$R''_{conduction} = \frac{L}{k}$$

where L is the component's geometric dimension (m) normal to the heat flux surface. Heat is ultimately transferred to the ambient surrounding via convection at the system boundary and results in the thermal resistance

$$R''_{convection} = \frac{1}{h_{ambient}}$$

This value is typically based on air with convection coefficients, h, ranging from $5 - 25$ or $10 - 200\frac{W}{m^2K}$ for natural and forced air convection, respectively. Radiation thermal resistance effects also exist, but can be often neglected for many system models.

For simplification, it is assumed that Daktari's joining process transmits energy *directly* to the intended bond interface. The parameters required to determine the steady state one dimensional heating profile of cuvette material for bonding directly at the interface is depicted in 4-6(a). The schematic is configured such that $R''_{cuvette}$

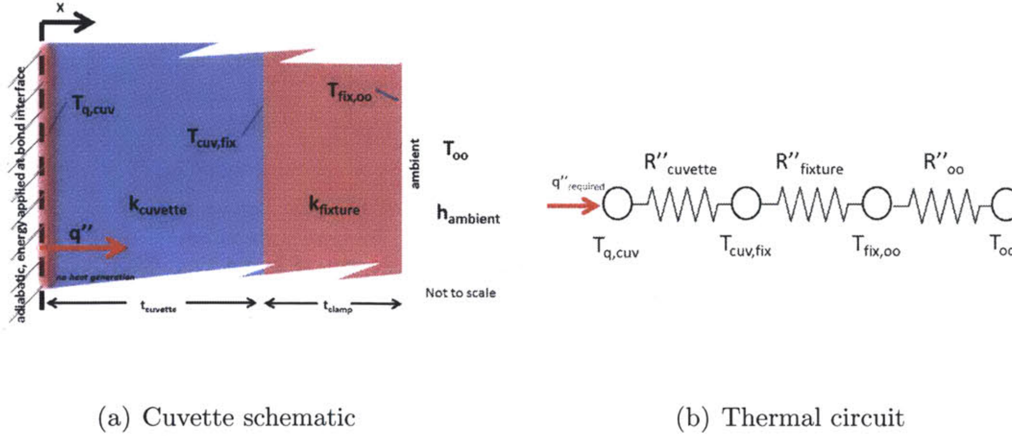

(a) Cuvette schematic

(b) Thermal circuit

Figure 4-6: Equivalent thermal circuit for the cuvette, a series composite wall with heating occurring at the bond interface

may be of either the lid foil or the microfluidic backbone component. This is a simplification that ignores the fact the heating from the weld interface outward cannot be properly observed as two independent halves of the entire system. However, it is assumed that the single direction of heat conduction emitting normal from the interface can be described as an adiabatic barrier across which heat will not flow and the following insights build from this simplification. Moving forward while acknowledging these limitations, the appropriate geometric and material parameters for the fixture configuration can be substituted depending on the region of interest. Thus the heat flux required is

$$\frac{T_{bond} - T_{\infty}}{R''_{cuvette} + R''_{fixture} + R''_{\infty}} \leq q''_{required} < \frac{T_{fail} - T_{\infty}}{R''_{fixture} + R''_{\infty}} \tag{4.7}$$

which can quickly provide a feasibility of bonding methods based on the tooling and heat transfer capabilities if the cuvette bonding and failure temperatures are known. For completeness, both the lid and backbone side shall be sanity-checked to confirm $T_{q,cuv}$ reaches T_{bond} and $T_{cuv,fix}$ does not result in deformation that fails to meet assembly requirements at T_{fail}. Using the present component configuration of

the cuvette and laser fixture, we can determine the minimum heat flux required to initiate melt of the lid at $x = 0$ after infinite time to reach equilibrium as

$$q''_{min,lid} = \frac{T_{bond,PMMA} - T_{\infty}}{R''_{lid} + R''_{fixture,BK7glass} + R''_{\infty}} = \tag{4.8}$$

$$\frac{200^{o}C - 28^{o}C}{\left(\frac{250\mu m}{0.19\frac{W}{m^2K}}\right) + \left(\frac{10mm}{1.114\frac{W}{m^2K}}\right) + \left(\frac{1}{10\frac{W}{mK}}\right)} = 1.560\frac{kW}{m^2}$$

It follows that for the backbone side minimum heat flux during steady state

$$q''_{min,bb} = \frac{T_{bond,PMMA} - T_{\infty}}{R''_{bb} + R''_{fixture,X5CrNi18-10} + R''_{\infty}} = \tag{4.9}$$

$$\frac{200^{o}C - 28^{o}C}{\left(\frac{2mm}{0.19\frac{W}{m^2K}}\right) + \left(\frac{15mm}{15\frac{W}{m^2K}}\right) + \left(\frac{1}{10\frac{W}{mK}}\right)} = 1.542\frac{kW}{m^2}$$

In this embodiment and in the steady state case, it takes slightly more heat flux to bring the lid to bonding temperature than backbone. As such, there is a presumed asymmetry in the HAZ within the lid compared to the backbone. Thus the backbone would have a larger HAZ than the lid for a given heat flux at the bond interface since the backbone would be experiencing more heating than required. Equation 4.10 shows a comparative HAZ ratio, $\bar{H}$, comparing q''_{min} for each component in the steady state condition

$$\bar{H}_{\frac{bb}{lid}} \equiv \frac{q''_{min,lid}}{q''_{min,bb}} \tag{4.10}$$

The ratio realizes a magnitude of a theorized HAZ asymmetry for the steady state simplification, with a $\bar{H}$ of unity being the symmetric HAZ case. With a negative correlation to $q''_{min,bb}$, values greater than unity have a greater backbone side HAZ compared to the lid side. If bonding and ambient temperatures are equal, we can further simplify and observe the positive correlation of larger backbone side thermal resistance, $\sum R''_{bb}$, to a larger backbone side HAZ.

$$\bar{H}_{\frac{bb}{lid}} = \frac{q''_{min,lid}}{q''_{min,bb}} = \frac{\sum R''_{bb}}{\sum R''_{lid}} \tag{4.11}$$

The relative magnitude of each of the thermal resistances in proportion to the total $\sum R''_t$s are outlined in the chart of Figure 4-7(a) and 4-7(b), with a more illustrative combined breakdown in Figure 4-8. It illustrates that the effect of the fixture resistance has a larger influence on the total resistance (and thus on q''_{min}) on the lid side since R''_{lid} is so small. It is presumed these proportions are very important factor in effective system thermal management, though R''_{fix} is more difficult to modify in present laser system. R''_{∞} is essentially a fixed boundary condition for normal ambient workplace conditions and has a very large effect on total system resistance in the steady state situation. However, this is only true since each thermal resistance is "felt" only after a sufficiently long time has elapsed and temporal gradients have ceased. In other words, the R''_ts far from the heating may not be instantaneously relevant to heating at the interface. However, the converse may be true for instantaneous temperature during cooling.

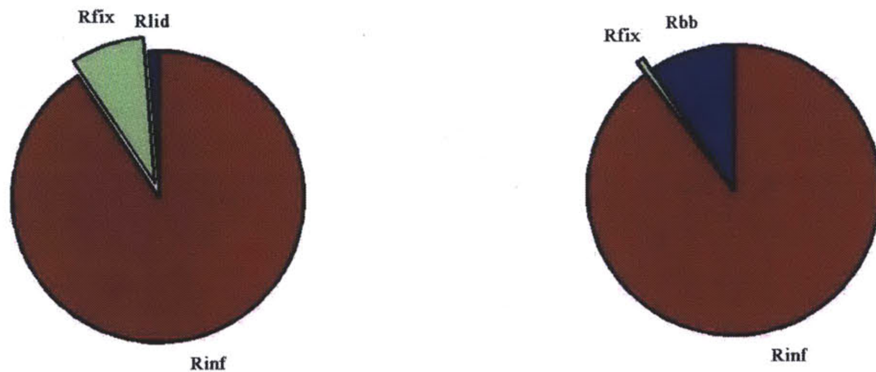

(a) Heat flow through the lid

(b) Heat flow through the backbone

Figure 4-7: Relative thermal resistances experienced by each system side in steady state compared to that side's total modelled thermal resistance

The literature shows that through transmission welding does result in asymmetric

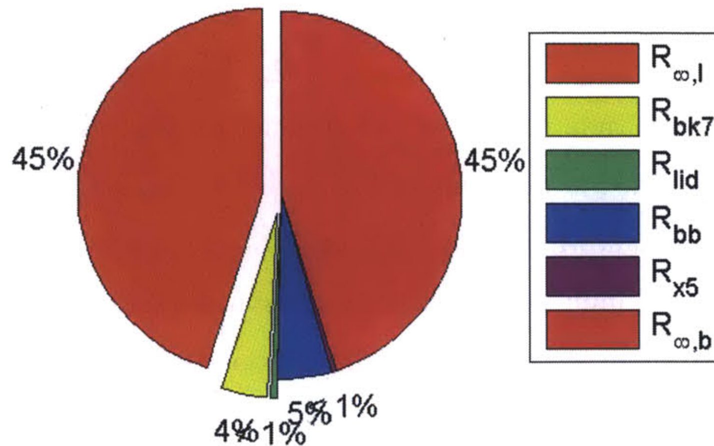

Figure 4-8: Breakdown of thermal resistances on each side of the cuvette. Resistances pertaining to the lid side are exploded. In steady state, $\bar{H}$ results in a nearly symmetric HAZ for the laser model

HAZ, as depicted in Figure 4-9(a)) as presumed in 4.11. [33] Considering the known issues of thermoplastic deformation listed in 2.3, engineering the thermal resistances to control the HAZ would be ideal. Furthermore, engineering the resistances could introduce a desirable asymmetry in the HAZ. If the HAZ is preferentially located on the lid side, it is theorized that backbone deformation from welding could be reduced. While still assuming equilibrium state, the described tuning potential is graphically shown in Figure **??** by plotting the minimum required heat flux in equation of 4.8 as R''_{fix} varies logarithmically while ambient conditions and material properties are held constant).

4.3.2 Contact Resistance and Pressure

The cuvette components are manufactured to the highest injection molding tolerances. Still, there are finite part geometric tolerances and finishes such that local sections of the bond interface may not be in perfect intimate contact. While we assume perfectly complementary surfaces for he simplification of the system in Figure 4-6(a), the contact resistance previously alluded due can significantly change the energy

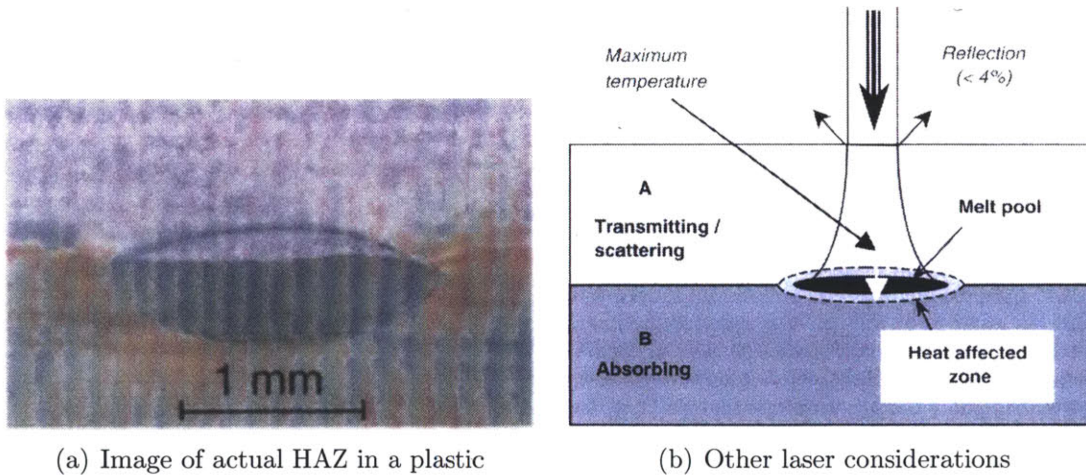

(a) Image of actual HAZ in a plastic

(b) Other laser considerations

Figure 4-9: Other laser considerations that affect the HAZ and actual image of heat affected zone. Degree of HAZ asymmetry is the result of non-ideal transmission, asymmetric thermal resistances and absorption, and transient temperature distributions

required to reach proper bonding temperature due to air gaps between component layers. Instead of creating a more complicated parallel resistive model of randomly sized and positioned air gaps, an average $R''_{contact}$ should therefore be accounted for in the series thermal resistance summation $\sum R''_t$.

It is documented that an increase in bonding pressures will encourage reptation and reduce the weld variability associated with finish sensitivities. [34] In addition to material intrinsic melt properties that are pressure dependent, high pressures encourage the intimate contact between join partners and effectively reduces $R''_{contact}$. As shown in Figure 4-10(a), a significant increase in lap shear strength is experienced for a given energy input as the residual gap approaches zero [33]. Actual part deformation or fixture compliance under clamping pressure may fill any residual gaps in the system to encourage good thermal contact would more effectively translates the bonding energy into heating the material to T_{bond}. While nominally beneficial for bond strength, it is unclear whether this pressure should be reduced to counteract channel deformation or inevitable internal stresses in the cuvette system at hand.

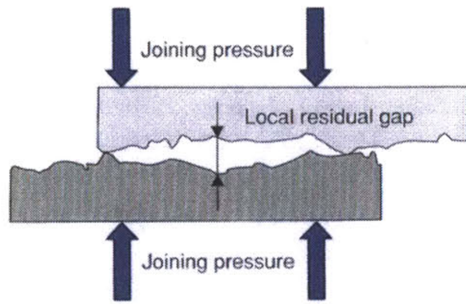

(a) Residual gap between join partners.

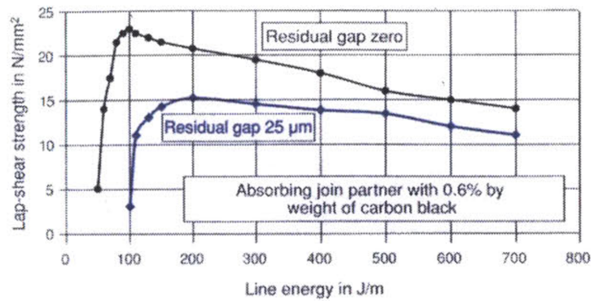

(b) Lap-shear strength of 2mm PP laser countour welded.

Figure 4-10: Effect of the residual gap on energy required for bond strength

4.3.3 Temporal Effects

Until this point, the qualifier *steady state* is emphasized in the simplified model of laser bonding. While the equilibrium case provides insight into the relative effects of thermal resistances and the absolute minimum q'' required to bond, the actual laser energy focal point is nominally travelling at $80\frac{mm}{s}$ around the weld path and the plastic has a short instance of laser exposure. Plastics have very steep and non-linear thermal gradients when subject to an impulse of heat energy. The dynamic response of the temperature profile is more appropriately depicted as in Figure 4-11(b). [73]

As such, R_t''s far from the weld interface may not be instantaneously relevant as the temperature changes diffuse through the system layers. Temporal temperature response insights are therefore gleaned by observing the actual laser welding process. While acknowledging that the laser beam spot is a Gaussian energy profile, we nonetheless assume uniform power passing into the welder's tunable weld spot diameter at the bond interface for the purpose of approximation. In accordance to experimentally determined best practices for focal depth, the spot size, D_{spot}, varies between $20\mu m$ to $40\mu m$. The intensity of normally incident light from the laser head at usual cuvette bonding operating power is determined by

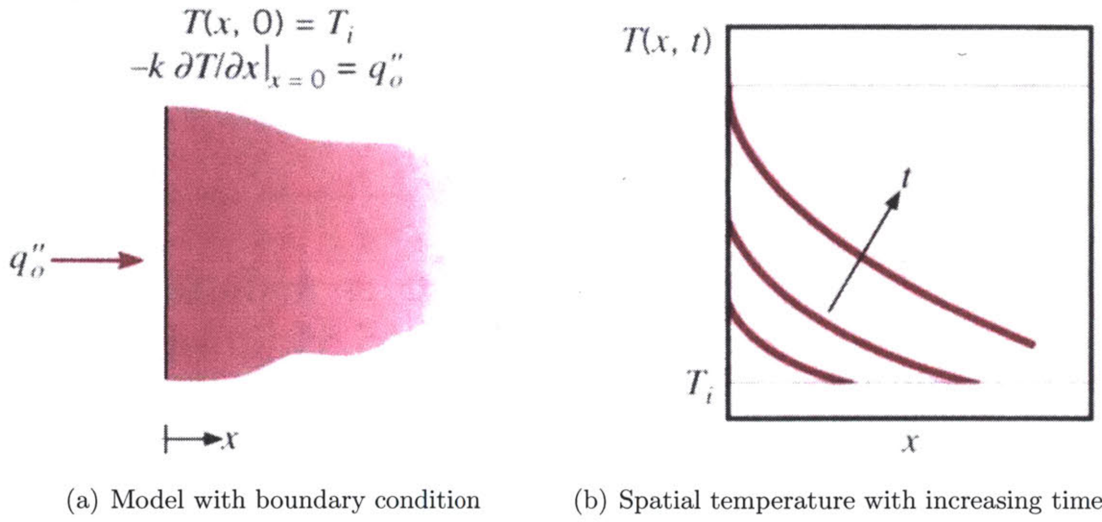

(a) Model with boundary condition (b) Spatial temperature with increasing time

Figure 4-11: Transient temperature distributions with gradients shown as a simplified semi-infinite solid for the constant surface heat flux boundary condition. Distance x increases through the cuvette component away from the bond region

$$q''_{laser} = \frac{P_{nom}}{A_{spot}} = \frac{8W}{\frac{1}{4} \cdot \pi \cdot D_{spot}^2} = 6,366 \ to \ 25,465 \frac{MW}{m^2}$$

According to Siegel and Howell, transmission laser welding energy intensity varies along its direct path as

$$q''_{laser}(x) = (1 - \eta)\, q''_{laser} e^{-Kx} \tag{4.12}$$

the laser light intensity as a function of distance from the transmissive part in units of $\frac{W}{mm^2}$. η is the surface reflection (%) of the transmissive part. K is the extinction coefficient in mm^{-1} and dependent on wave absorption and scattering factors. Though parameters for the materials at study were not available at the time of writing, using comparable plastic values we can visualize the dependences heat flux has on depth into the part and as K increases in Figure 4-12. [74] Transmitting through the $0.25mm$ lid, this corresponds to the laser imparting about $10,000\frac{MW}{m^2}$

at the intended weld interface. Crude approximation aside, the laser is more than capable of conveying enough energy for the bond interface to reach T_{bond} compared to the steady state minimum in Equation 4.8. This is corroborated by empirical evidence; testing shows that short instances of laser exposure are required to prevent burning of the weld.

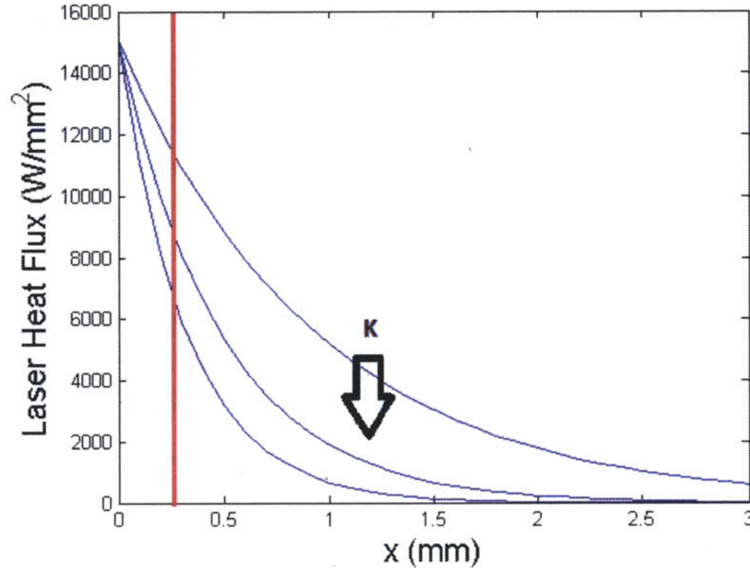

Figure 4-12: Heat flux of the laser, q''_x, as a function of distance from the laser-transparent component top towards the weld interface at the absorptive component. Heat flux dependency on extinction coefficient, K, also illustrated

Further qualifying temporal factors, part geometry is taken into account with the component's *characteristic length*

$$L_c \equiv \frac{V}{A_s}$$

which is the ratio of the solid's volume, V, to surface area, A_s. It should be associated with the length scale corresponding to the maximum spatial temperature difference (for a symmetrically heated plane of wall thickness $2L$, L_c would remain the half thickness L, as utilized in our model). Recall the heat equation parameter for thermal diffusivity, α. α can alternatively be described as a measure of a material's

ability to conduct thermal energy relative to storing it, its thermal inertia. α and L_c are used together with time, t, to form dimensionless thermal time response. The *Fourier number*

$$Fo \equiv \frac{\alpha t}{L_c^2} \tag{4.13}$$

is ratio of the heat conduction rate to the rate of thermal energy storage. Since most plastic welding methods take place on time scales where spatial gradients in time cannot be ignored, a more nuanced and non-linear time varying heat transfer results. The non-dimensional *Biot number*

$$Bi \equiv \frac{R_t''}{R_{surround}''} \tag{4.14}$$

provides a measure of the temperature drop in a solid relative to its surrounding, where the $R_{surround}''$ material envelopes the material with R_t'' that is the focus of the time heat transfer study. For the special condition of $Bi < 0.1$ it is reasonable to assume a uniform temperature distribution across the solid at any time during a transient process. This would be applicable to thin metal implants in temperature sensors or heating elements embedded in a high R_t'' plastic surround, such as

$$Bi \equiv \frac{R_{thinmetal}''}{R_{surround}''} = \frac{\frac{L_{c,thin}}{k_{metal}}}{\frac{L_{c,1000\times thin}}{k_{plastic}}} << 0.1$$

While the thin metal will have no spatial gradient over time (and assumed throughout this work), the PMMA thermoplastic cuvette components to be bonded frequently have a Bi that becomes $>> 1$. These high Biot situations mirror the system schematics of Figure 4-6(a) when the plastic is surrounded by ambient air, other plastic components, or more thermally massive metals (such as the fixtures at hand) that causes steep thermal gradients in time (reiterated in Figure 4-13(a)). The Biot number gradient illustrates some of the discrepancy in steady state heat flux in the simplified model and the higher fluxes over shorter time intervals in practice.

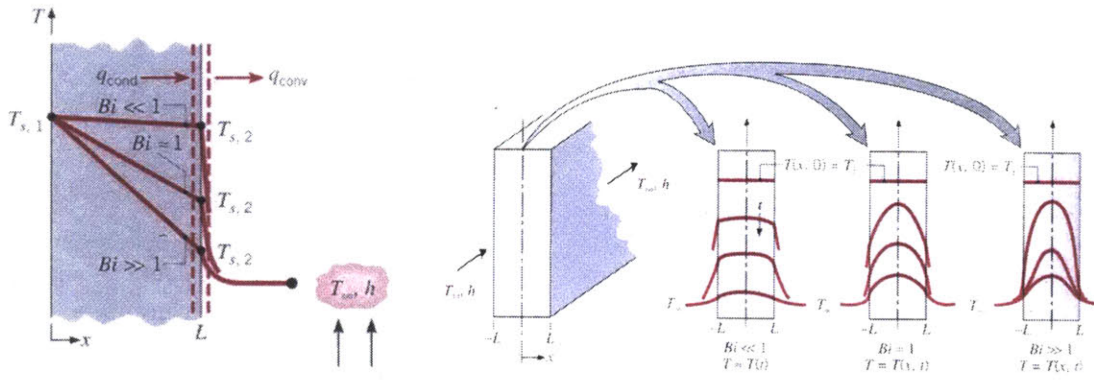

(a) Effect of Biot number on steady-state temperature distribution in a plane wall with surface convection

(b) Transient temperature distributions for different Biot numbers in a plane wall symmetrically cooled by convection

Figure 4-13: The effect of the non-dimensional Biot number in solids relating the spatial gradients of temperature in a solid relative to its surrounding

Together, the Fourier and Biot dimensionless numbers characterize transient conduction problems. These forms are utilized in analysis with step temperature inputs in uniform Newton heating or cooling, having analogous solutions to RLC electrical circuits and control theory. Each material in the system under study has a temperature response to the thermal input that will determine the non-linear spatial temperature gradient as well as time constant (τ) to reach 63.2% of its final (asymptotic) value if it indeed approaches steady state. Unfortunately, closed form approximations such as the *lumped capacitance* or *semi-infinite solids* are problematic since the boundary conditions of all three dimensional surfaces are so close in the actual microfluidic embodiment that edge effects, heat transfer rates, and temperature profiles in both realistic time scales and dimensional space are interrelated.

4.3.4 Advanced Modelling

Advanced modelling and analysis can provide insight to the dynamic temperature at different distances from the location where energy is generated. This is particu-

larly important at locations within the cuvette part that need to reach T_{bond} while other locations require remaining below the temperature of failure. Transient effects determine how quickly the temperature front reaches a given point in a cuvette system that experiences steep and non-linear thermal gradients during the short welding time. Recall that thermoplastic T_g is a regime dependent on instantaneous system conditions, while required energies per volume resulting that cause failure and deformation are often only determined experimentally (Section 4.2.1). The instantaneous density, thermal conductivity, volumetric thermal expansion, and heat capacity vary non-linearly with temperature, local pressures, stresses and strains. Temperature and consequently HAZ profiles are complicated by experiencing a variety of materials thermal loads as the heat front expands outward. Apart from benchmarking with these simplified versions of transient and spatial heat gradient solutions, finite-difference or finite element methods are required to accurately model the time-dependence of temperatures and boundary heat rates of solids, usually necessitating computer based numerical solutions or multi-physics modelling software.

While potentially inaccurate, the aforementioned simplifications of analytical solutions nonetheless provide insight to the general driving physics of many thermoplastic microfluidic thermodynamic and heat transfer situations. Alternatively, research has demonstrated that with the appropriate equipment, actual welding dynamics can be recorded and correlated with multi-physics modelling visualizations. For instance, infra-red thermography can image spatial thermal gradients in time for certain configurations in which there is a clear and representative IR view path. [75] Additionally, Yi demonstrates that multi-physics solutions can accurately model the dynamic temperature profile of a PCR micro heater made of thin conductive elements in comparison to experimental observations (Figure 4-14). [76] A more complete review of laser modelling efforts correlated to joining data is available in the literature. [74, 77–80]

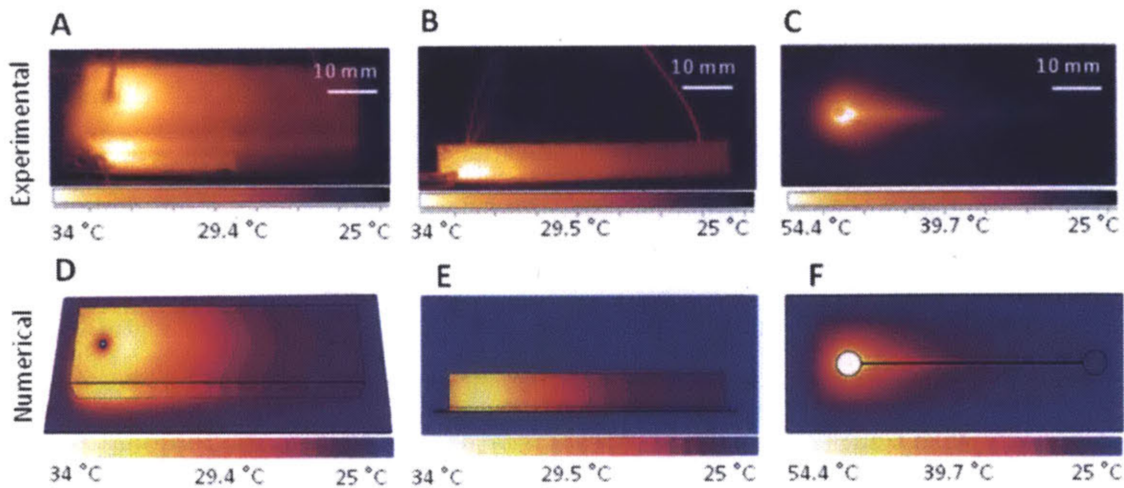

Figure 4-14: Temperature distribution across the external surfaces of the microfluidic system recorded with IR camera and compared to multi-physics simulations. DI water heated at the inlet with a resistive heater at a flow rate of $40\frac{mL}{min}$

4.4 Lessons from Laser Heating

While, laser welding expertise is external to Daktari, heat transfer parameters illustrate the relevant factors in exposing the intended weld joint to a high concentration of energy for a short amount of time. A minimum steady state q'' is derived based on material thermal resistances. This bounds our temporal analysis and, when balanced with production cycle time requirements, provides an objective to reduce weld deformation by not imparting more energy than necessary. Asymmetric R_t''s may be engineered in the system fixture to bias the HAZ away from sensitive areas while still providing a region for reptation that meets bonding requirements. Reconfiguring the assembly such that the backbone is transmissive and the lid absorptive may be another design option. While laser welding may have limitations, it is recognized that other processes could exploit the cuvette's sensitivity to its surrounding fixture.

Whatever the method of analysis, the intuition of the relevant welding effects shall drive subsequent testing and engineering design to develop a heating process solution. Daktari's cuvette has demanding geometrical tolerances that continues to

push the limit of what is possible for LOC thermoplastic welding. The rest of this thesis will build from the lessons learned in Chapters 3 and 4 in the development of a method of heating conductive implants. This is a manufacturing R&D exercise that can be rapidly iterated in a short time frame thanks to Daktari's electrode production process.

Chapter 5

Heating Thin Implants

Preliminary testing and research in Chapters 3 has shown the utility in heating a thin film implant for the welded cuvette assembly step and perhaps other LOC applications. With the knowledge of the mechanics necessary to bond thermoplastics outlined in Chapter 4, we explore the capabilities of Daktari's proprietary flexible and robust sensing electrode production process applied to creating conductive patterns that usefully heat micro-features in on the product. Benefits of working with the conductive implants include the ease of characterizing the energy imparted since it is based on simple electric phenomenon in addition to the fact that welding with implants is not dependant on material color, as opposed to the absorptivity requirements in laser methods.

5.1 Properties

The manufacturer of the material used in Daktari's electrode production process discloses nominal material properties. The process is thus able to create conductive patterns for implants with the generalized geometry of Figure 5-1

Resistance, R, in units of Ohms (Ω), is a property of the conductor material and determined by *Pouillel's Law* with cross section $\widehat{A}$:

$$R = \bar{\rho}\frac{l}{\widehat{A}} = \bar{\rho}\frac{l}{wh} \tag{5.1}$$

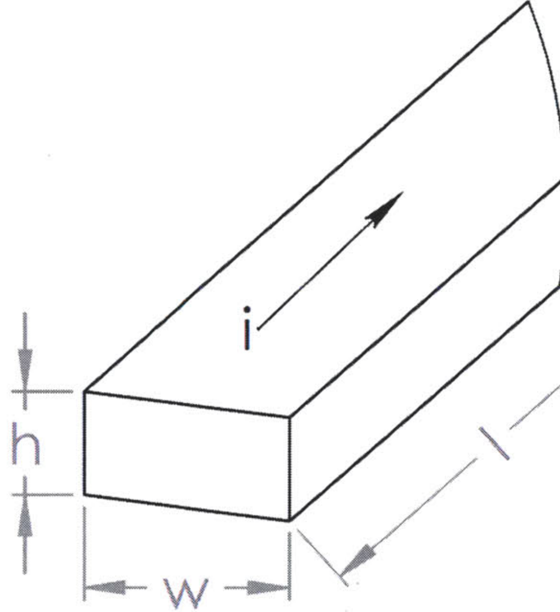

Figure 5-1: Implant cross section (not to scale).

Resistive heating is the process by which the passage of an electric current through a conductor releases heat. For the resistive implant with constant direct electric current, i, in units of amps (A), electrical energy is generated at a rate of

$$\dot{E}_g = i^2 R = i^2 \bar{\rho} \frac{l}{wh} \tag{5.2}$$

in units of Watts (W). Assuming operation at the maximum rated current density in the direction normal direction of current flow is J_{max}, we substitute to find the maximum possible energy generated as listed by the manufacturer for a given geometry

$$\dot{E}_{g,max} = J_{max}^2 \bar{\rho} whl \tag{5.3}$$

We abstract geometric factors and determine the volumetric energy flux, $\dot{q}$, by dividing by the implant volume, V,

$$\dot{q} = \frac{\dot{E}_g}{V} = \frac{\dot{E}_g}{lwh} = \frac{i^2 \bar{\rho} \frac{l}{wh}}{lwh} = \frac{i^2 \bar{\rho}}{(wh)^2} \tag{5.4}$$

in units of $\frac{W}{m^3}$. Substituting for known values, we determine the maximum manufacturer rated volumetric heat flux

$$\dot{q}_{max} = \frac{\dot{E}_{g,max}}{V} = J^2_{max} \bar{\rho} = 5.043 \times 10^9 \frac{W}{m^3} \tag{5.5}$$

$\dot{q}_{max}$ can be used to set current limits for a desired implant geometry. However, it should be noted that $\bar{\rho}$ is a function of temperature and the geometric dimensions have finite tolerances. It would be useful to know the methods from which the manufacturer specifications were derived, since the maximum listed power rating, $\dot{E}_{g,max}$, does not correlate to the geometry dependant volumetric heat flux in 5.5. However, this is manufacturer proprietary information. Future collaboration with the vendor is required to progress development of their material and process.

5.2 Feasibility

For testing, implants were created of various lengths and shapes in order to characterize the heating process. Typically, the cross section h was $2600\mathring{A}$. The implant thickness has no documented tolerance known, though it is qualitatively observed as relatively variable since it is at the limit of the material manufacture process capability. The width w of the section to be heated was held at approximately $0.06in$ based on initial experimental trials of the process, though this dimension is somewhat arbitrary. If found to be inadequate, the w dimension can be held to tighter tolerances. The initial experimental implant geometry is shown in Figure 5-2(a).

For the geometry of the initial experiments with an L of $1.5in$, Figure 5-3 demonstrates the J and $\dot{E}_g$ of 5.2 as a function of input i.

There is a linear dependency on the length of the implant for the generated energy, as indicated by the curves, with l increasing from the initially tested case. For the $1.5in$ samples initially tested, the power limit according to J_{max} would be

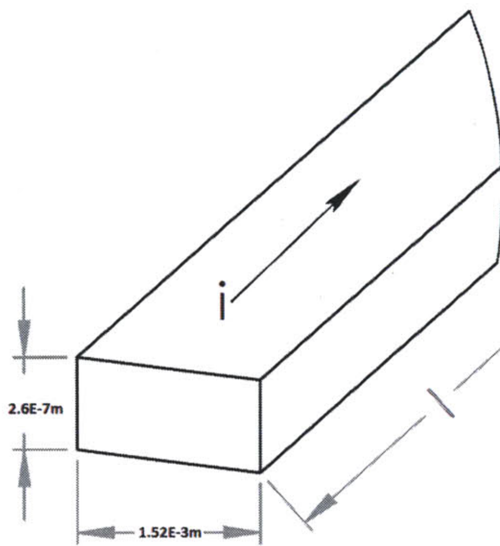

(a) Schematic

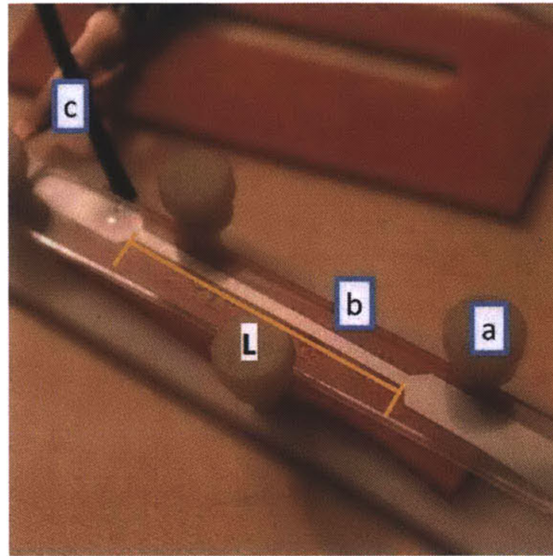

(b) Initial test

Figure 5-2: Experimental implant initial tests and schematic. The cross section was held at the listed nominal values. Length, L, is dependent on the particular test and in the simplified initial tests was $1.5in$

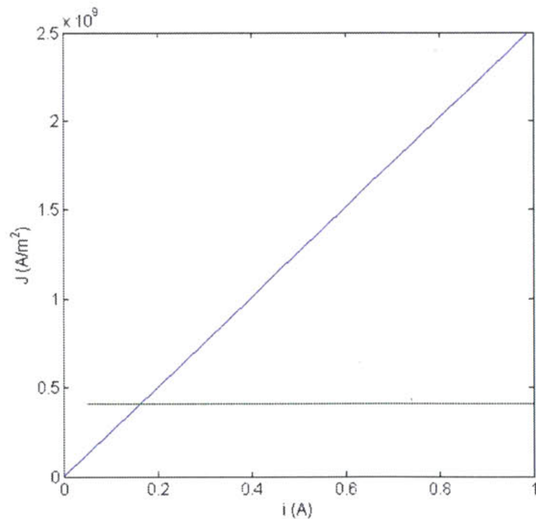

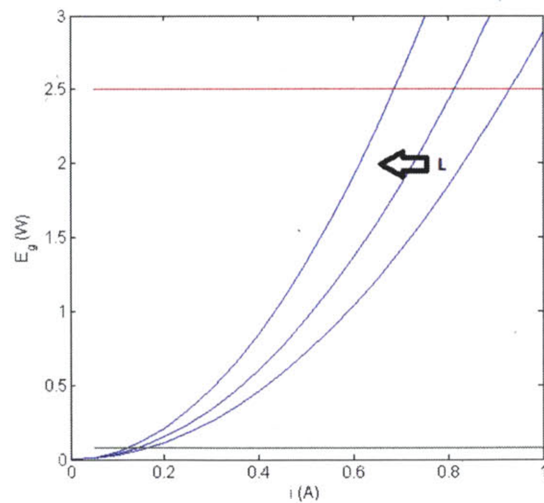

Figure 5-3: On left, current density versus current for the tested cross section with manufacturer maximum indicated. On right, energy generated versus current with the aforementioned current maximum configuration as well as $\dot{E}_{g,max}$ indicated

$$\dot{E}_{g,max}(l = 1.5in) = J_{max}^2 \bar{\rho} whl = 0.076W \tag{5.6}$$

and indicated in the plot in Figure 5-3. Interestingly, the $\dot{E}_g$ derived from the maximum current density does not correlate to the rated $\dot{E}_{g,max}$ of $2.5W$, making the efficacy of the provided material specifications questionable. (*N.B.* $\bar{\rho}$ increases with temperature which is interrelated to the total $\dot{E}_g$. A more complicated generated power curve exists when incorporating this detail.) The steady state thermodynamic model of Section 4.3.1 can also be applied to the cuvette when heated with an embedded implant. Figure 5-4 shows the cuvette with embedded conductive material exposed to an ambient directly (no fixture resistance in model).

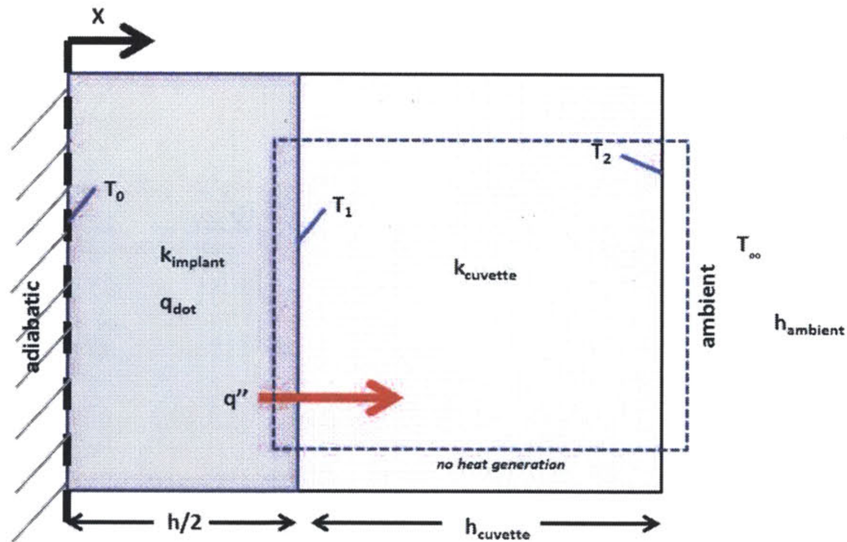

Figure 5-4: Thermal model of an implant generates energy ($\dot{E}_g$) symmetrically embedded between cuvette components and exposed to the ambient

Since the surface at $x = 0$ (at the center of the implant thickness) is assumed adiabatic, there is no inflow at this location and the rate at which energy is generated

must equal the outflow. We ignore edge effects since $w >> h$ and observe a one dimensional heat equation (4.4) collinear with the h direction (or x direction in Figure 5-4). Accordingly, the heat flux per unit surface area is

$$q'' = \dot{q}\frac{h}{2} \tag{5.7}$$

To determine a first order feasibility of heating the implant between cuvette based on manufacturer ratings (the more conservative J_{max} value), we determine heat flux capability

$$q''_{max} = \dot{q}_{max}\frac{h}{2} = \left(5.043 \times 10^9 \frac{W}{m^3}\right)\frac{2600\mathring{A}}{2} = 656\frac{W}{m^2} \tag{5.8}$$

With the qualifier that the following plots are only numerically valid for constant $\bar{\rho}$ and if edge effects can be neglected in the specific geometric configuration at study, Figure 5-5 illustrates the exponential increase in $\dot{q}$ and q'' of equations 5.5 and 5.7, respectively.

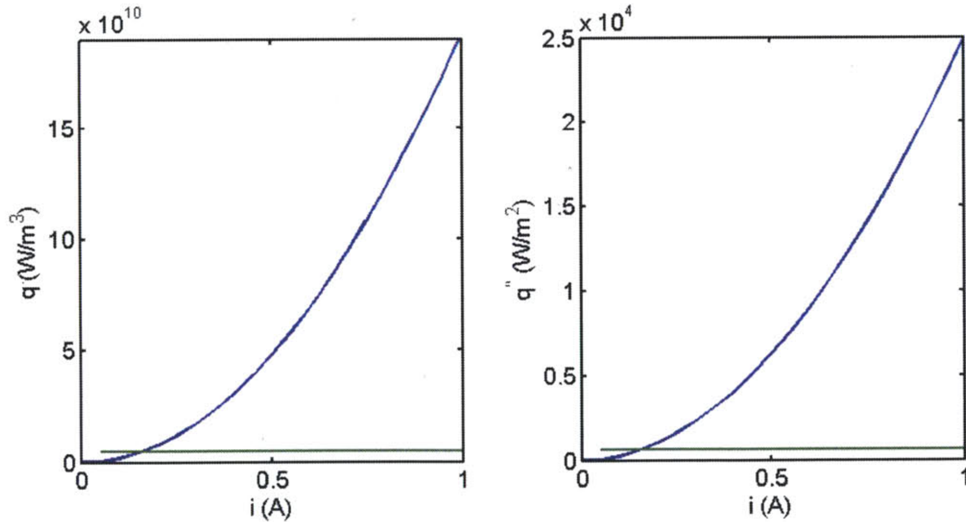

Figure 5-5: On left, predicted volumetric heat flux of the implant with manufacturer maximum indicated. On right, heat flux flowing normal to the bond interface, with rated maximum indicated. The curves are identically shaped with a difference in scales attributed to a factor of $\frac{1}{2}h$

This is within the sensitive region of the minimum required heat flux for the cuvette, depicted in Figure ??. It is therefore predicted that the success of welding by heating the implants that can be created with Daktari's electrode process will be similarly sensitive to, and dependant on, the thermal resistances, R_t''s, of the welding clamping fixture. Therefore, testing of different embodiments of the trapped implant between the cuvette components with a clamping fixture is required.

5.3 Experimental Performance

Even though the rated parameters of the material predict a heating power that would be very sensitive to fixture thermal resistances in the ideal steady state case, experiments nonetheless demonstrate substantial heating and melting of the PMMA lid. The straightforward application of DC power to the implant quickly exhibit that an element can reach T_{melt}. Figure 5-6 shows the preliminary experimental setup to bond clear PMMA.

Figure 5-6: Preliminary desktop experimental setup with $15V$ $3A$ power supply, handheld thermocouple thermometer, and PMMA bonding jig

By increasing the voltage, V, on the power supply in steps and observing the steady state current output, we can roughly estimate the power, P, dissipated in the implant by using *Joule* heating

$$P = Vi = \dot{E}_g \tag{5.9}$$

Joule heating is equivalent to $\dot{E}_g$ in Equation 5.2 (and thus also known as the aforementioned resistive as well as *ohmic* heating). The implant is not a perfect *ohmic* resistor in the temperature range on which it operates. Equation 5.9 is an alternative form of $\dot{E}_g$ that acknowledges R is not constant and utilizes the power supply output parameters V and i to determine P.

A sample representative of the cuvette was created by sandwiching the conductive implant between a $2mm$ featureless mock backbone and a production $250\mu m$ lid. The test assembly was placed in a simple fixture (originally used for inductive feasibility tests in Section 3.4.2) with a spare piece of $\frac{1}{8}''$ silicone to more evenly distribute the thumb screw pressure and ensure the mock backbone and lid were preloaded in intimate thermal contact, according to Section 4.3.2. Figure 5-7(a) demonstrates the generated power in these initial tests.

The energy is dissipated in the PMMA as heat, producing a direct PMMA to PMMA bond region adjacent to the implant. The process is susceptible to hotspots and fuse-like failure mechanisms that beak continuity and interrupt heating. This may a result of uneven clamp pressure resulting in variable $R''_{contact}$ and unintended heat buildup. Either thermal expansion stresses or material defects result in a smaller effective cross section that increases J. Run-away local heating ensues, resulting in failures at an identifiable locus. Regardless, it is demonstrated that close to $3W$ can be sustained before the breakage of continuity, a power value actually greater than the rated $\dot{E}_{g,max}$.

Subsequent testing demonstrated the utility of observing the current draw over time for a fixed electric potential. This voltage was applied as an impulse and selected based on what the pattern seemed to sustain when slowly ramping the voltage upward

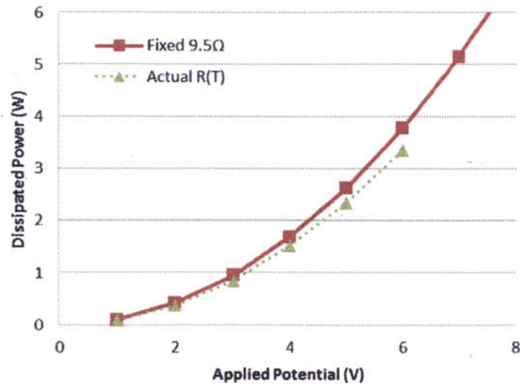

(a) Theoretical and actual dissipated power

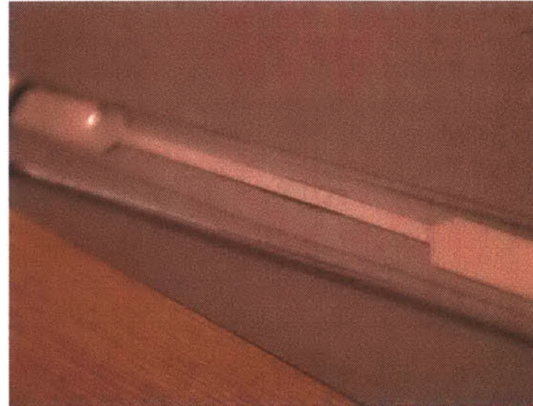

(b) PMMA bonds at a local hotspot. The failure ultimately breaks continuity and heating ceases

Figure 5-7: Initial implant trials prove the feasibility of heating with direct current. The power dissipated is less than a perfect ohmic resistor since the material resistance increases with temperature as the implant is heated by an applied electric potential from power supply. There are issues with failures at hotspots

until failure in prior testing. As the temperature increases in time, the implant resistance increases and dissipated power decreases. Figures 5-8(a)-5-8(f) provide an intuition to the implants response during the heating process.

Of note, the temperatures recorded are actually sensed at a heat sink on the pattern that was intended to be isothermal based on an erroneous Biot assumption (Section 4.3.3). Since welding was achieved, temperatures must have reached above $T_{bond,PMMA}$ at approximately 150^oC. The measurement therefore is not completely representative. In addition to the difference in the sensor location compared to earlier isothermal Biot analysis, there is less ohmic heat dissipation in the sensor location because it has a larger local cross section (lower J) and is thus a cooler spot. Subsequent testing was carried out with a modification of this sensing pad. Electrical contact of the thermocouple section from the intended heated implant was broken and lid material was removed such that the sandwiched thermocouple did not contribute to defects. Thermal grease was added to more closely couple the thermocouple sen-

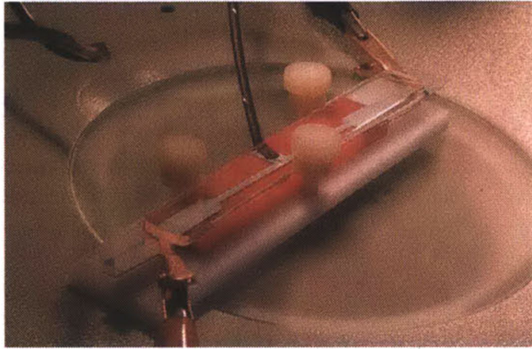

(a) Experimental setup

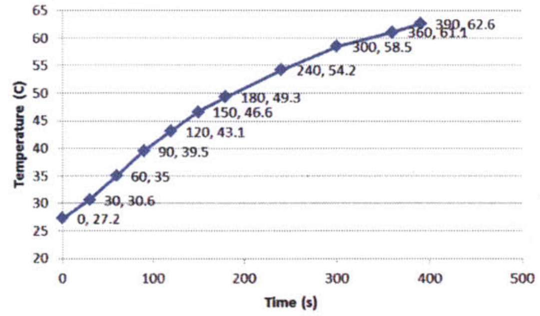

(b) Temperature versus time

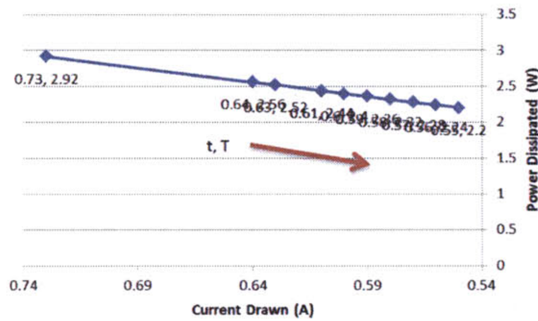

(c) Power versus current

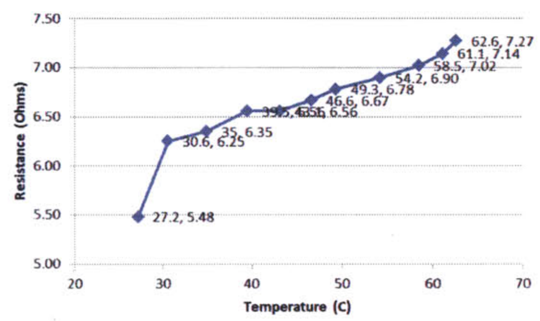

(d) Resistance versus temperature

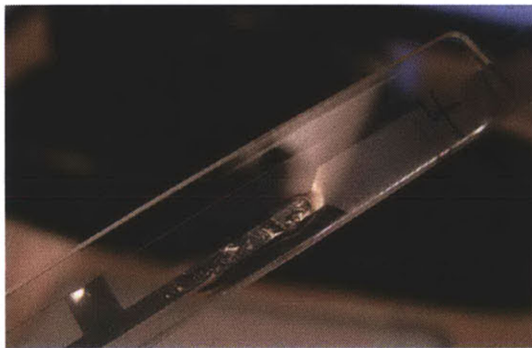

(e) Resultant sample under studty

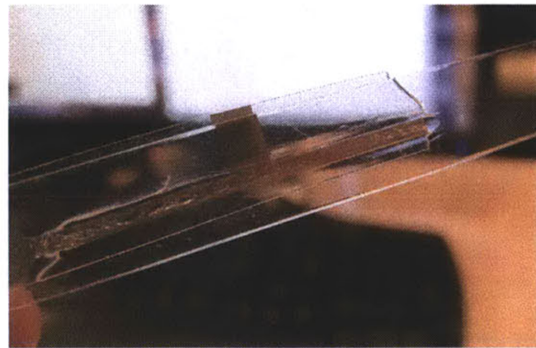

(f) Manual peel breaks lid material rather than weld

Figure 5-8: Data taken during initial testing provided insight into operational variables during implant bonding with a fixed power supply electric potential

sor to the actual interface temperature. The modified thermocouple placement and resultant high reading of 109.8^oC at $3min$ (though welding still occurs) is shown in Figure 5-9(a). If we assume this was still in a linear non steady state regime, the heating rate at the sensed location starting from room temperature is almost $0.5\frac{^oC}{s}$. A more careful derivation of τ for both heating and cooling response of the conductive implants is desired but requires further testing.

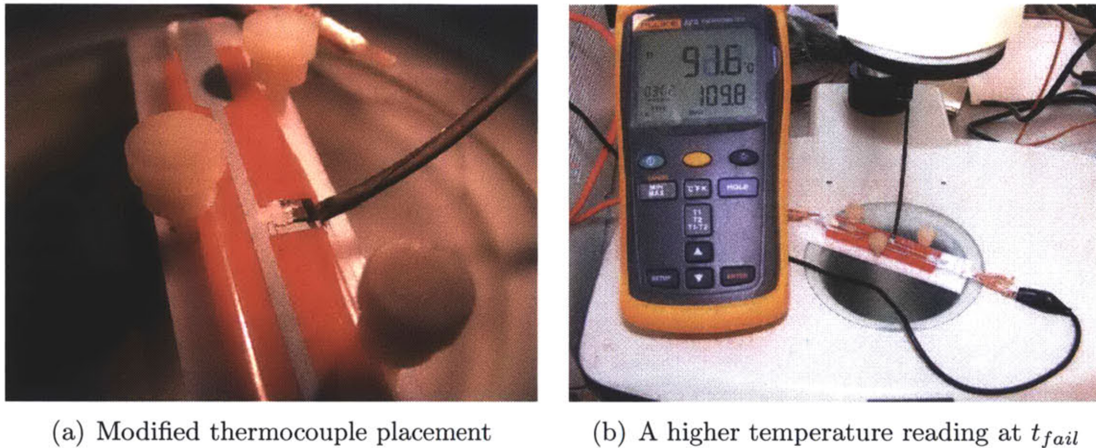

(a) Modified thermocouple placement (b) A higher temperature reading at t_{fail}

Figure 5-9: Modifying the thermocouple placement results in a more realistic temperature reading of the PMMA bonding that occurs

While initially unintentional, varying the trace geometry in such a way can be advantageously utilized to change J, and thus the dissipated power, in order to tune the temperature profile and weld HAZ at a location around the cuvette weld, shown in Figure 5-10(a). This method has analogy to engineering the bounding fixture thermal resistance proposed in Section 4.10.

Further insight into the dynamic parameters in welding the conductive implant are realized by recording temperature and power when i is held constant. A different power supply was utilized to provide a fixed current up to $1A$. Since potentials across the implant did not exceed $10V$, the voltage change of the welding process to be measured with an inexpensive data acquisition device (DAQ), illustrated in Figure 5-11(a). Assuming negligible losses at the trace leads or the wiring, the dominant

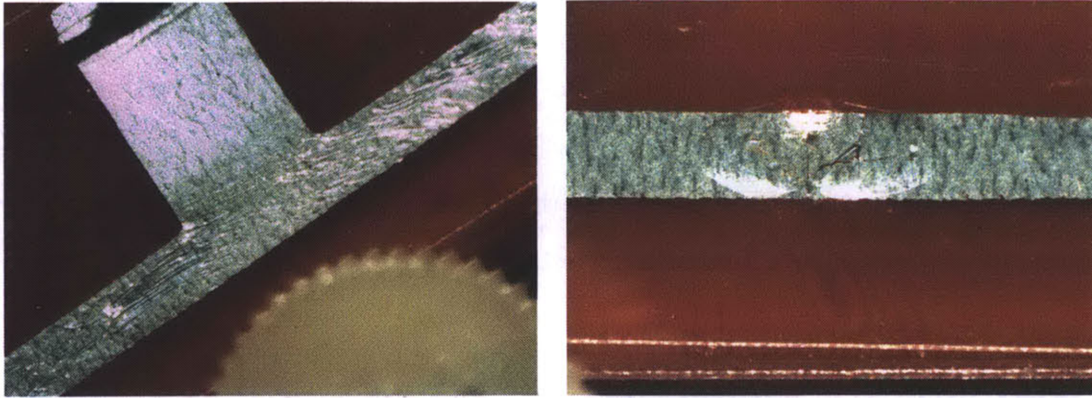

(a) The lack of implant wrinkling around Tc location is indicative of that region being cooler

(b) Fuse-like failure at hotspot J runaway

Figure 5-10: Nuances in dealing with the conductive implants

heat flux can be determined according to 5.7. The heat flux of this system is the measured power dissipated divided by the ohmically heated volume times the half thickness, h, of the susceptor in the direction of heat flux away from the intended bond interface, or

$$q''_{actual} = \frac{P}{2lw} \tag{5.10}$$

For the system at hand, this results in about $20,000\frac{W}{m^2}$ in the direction normal to the weld interface. This number is for the entire trace length area and is not for just a differential section, and thus is not directly comparable to the laser. Regardless, the temperature rise correlates to an almost 40% increase in R. Larger mock samples were fabricated and thin film T type thermocouples were utilized such that a more sensitive and responsive measurement would be recorded. The thermocouple was now positioned between the lid and the silicone directly below the implant in the initial fixture, as depicted in Figure 5-11(a).

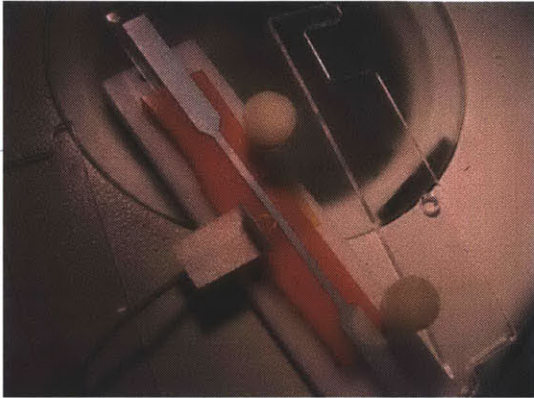

(a) Thin thermocouple can be sandwiched

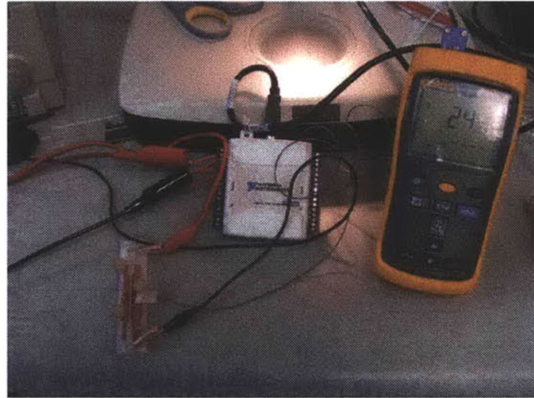

(b) Setup with thin film T type Tc and DAQ

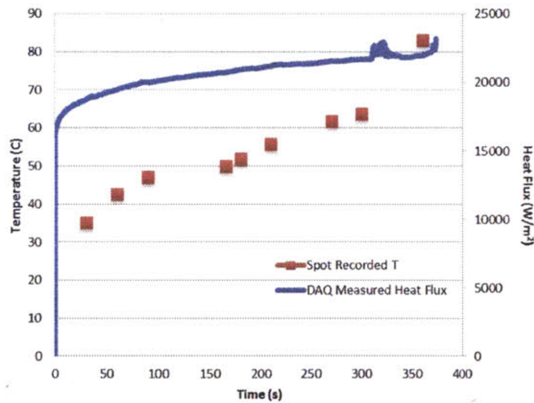

(c) Heat flux and temperature in time

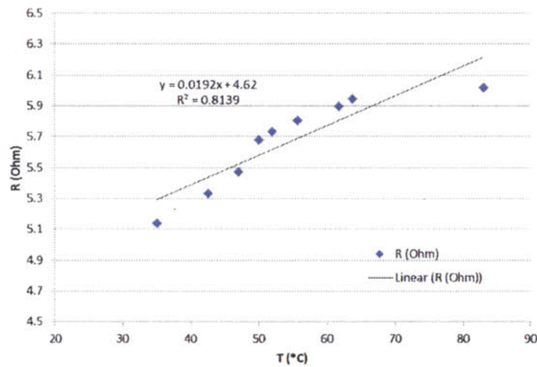

(d) Implant R versus T ($R_0 = 4.6\Omega$)

Figure 5-11: Testing with the DAQ and constant current power supply provides further characterization of the welding temperature and power response and a correlation between temperature and resistance

5.4 Welding Fixture

With an understanding of the required electric power and other nuances of welding the mock transparent PMMA cuvette assembly, a refined welding jig was designed that could handle full Daktari backbones, shown in Figure 5-12(a). System parameters such as bond time, heat flux, and pressure are still variables to be adjusted. The process cycle time should be decreased to facilitate the iteration of parametric study in order for the implant welding process to approach control. Properly constrained assembly locating features and toggle clamps allow for fast and repeatable user loading, especially with respect to electrical connection to the implant. Ideally, as the process is refined, the fixture will be future proof. It should be capable of both the aforementioned mock bonding directly to lid test substrates as well as pressurized operation with functionalized production electrodes. A final experimental utility of a transparent clamp allows the operator to observe and record the bonding in real time, a benefit that has shown to be invaluable to both the development of the implant heating process as well as general cuvette welding, including laser methods. Design for single fixturing and simple tooling paths with the use of off-the-shelf components encourage the welding fixture to be operational in short order and at low cost.

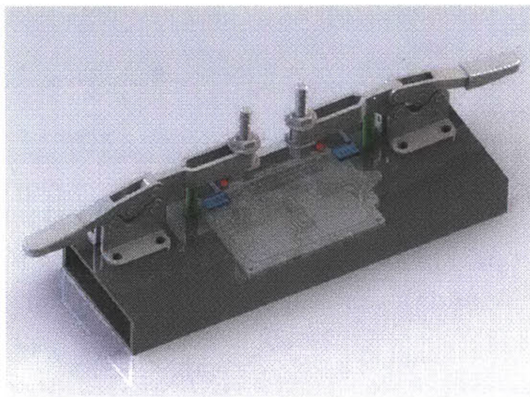

(a) Fixture as initially modelled

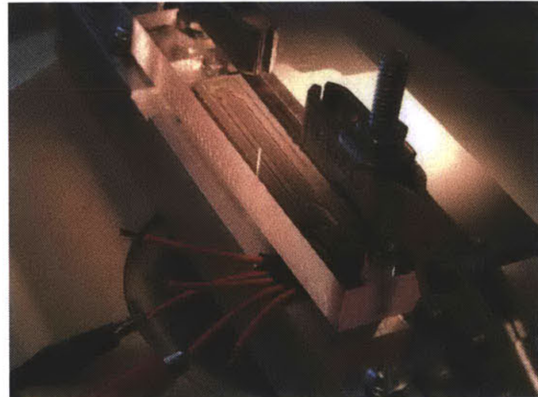

(b) Completed welding fixture with assembly

Figure 5-12: Fixture design and implementation

5.4.1 Thermal Resistance Issues

Repeated testing with the new fixture at higher than typical power levels did not produce bonds for the same test parts as the original fixture. At heat fluxes that would normally cause the implant to fail in the old fixture caused no response in the new design. Only after leaving the power on for an extended time did a bond occur. Unfortunately, the lid bonded to the polycarbonate clamp rather than the backbone (depicted in Figure 5-13(a)). This indicates a skewed HAZ to the lid side (as alluded in 4.11) such that the backbone never reached T_{bond} for reptation to occur between it and the lid. Instead, the lid side and PC clamp reached a weldable state as evidenced by a resultant bond that left remnants of the implant on the PC clamp after the lid was destroyed in manual peeling. Interestingly, $T_{bond,PC}$ is slightly greater than $T_{bond,PMMA}$. For consolation, the backbone was not deformed.

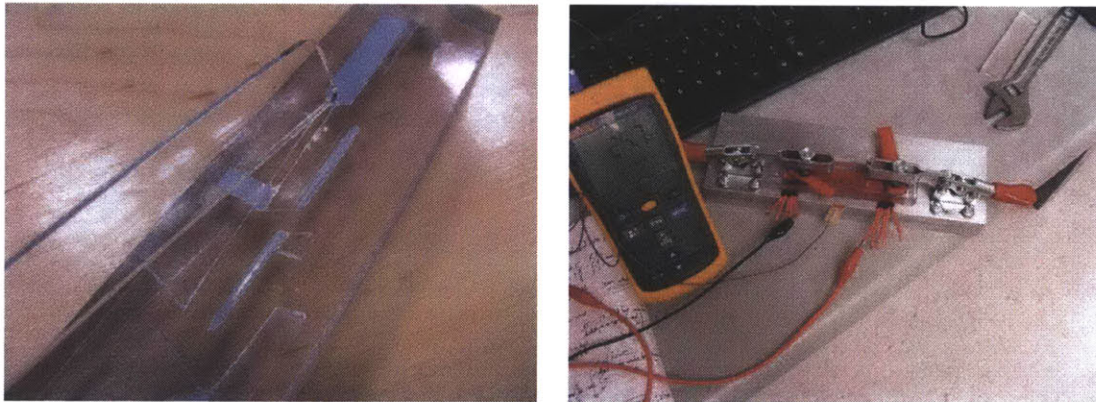

(a) Implants successfully heated but unintentially bonded directly to PC fixture clamp

(b) Bonding also failed when modifying the thermal resistance with fishpaper and silicone

Figure 5-13: It is apparent that the thermal resistance balance is an issue in the lack of welding. Even with the modification of the new fixture with fishpaper and silicone insulators, no bonding occurs. The aluminum bulk temperature of the fixture was observed to increase a few degrees

Adding a layer of insulative fish paper and silicone helped, but still did not accomplish bonding as demonstrated with the earlier fixture. Since heating was occurring

over a long period of time without failure, the new fixture was analyzed with the thermal resistance models developed in Section 4.3. Incorporating the new R_t''s, the relative contributions of each component relative to the total thermal load is shown in Figure 5-14(c).

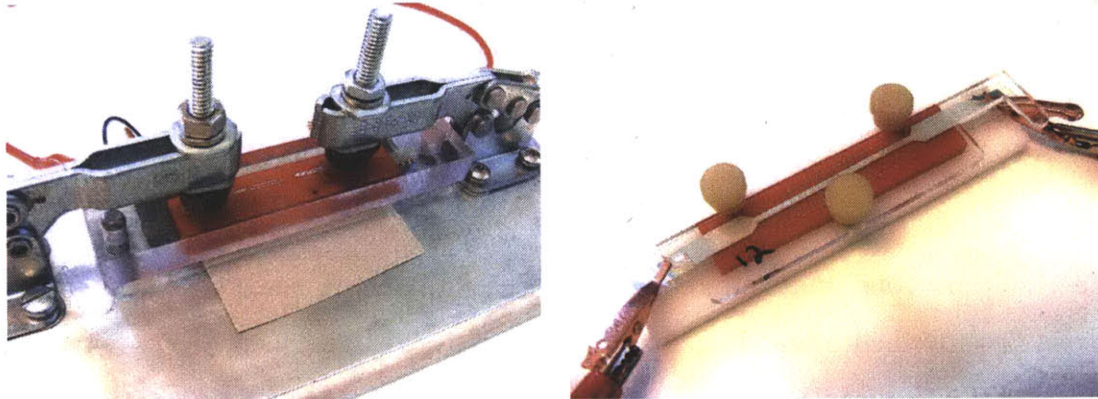

(a) New fixture with additional insulators did not weld the cuvette assembly

(b) Original fixture that successfully demonstrated welding with identical samples

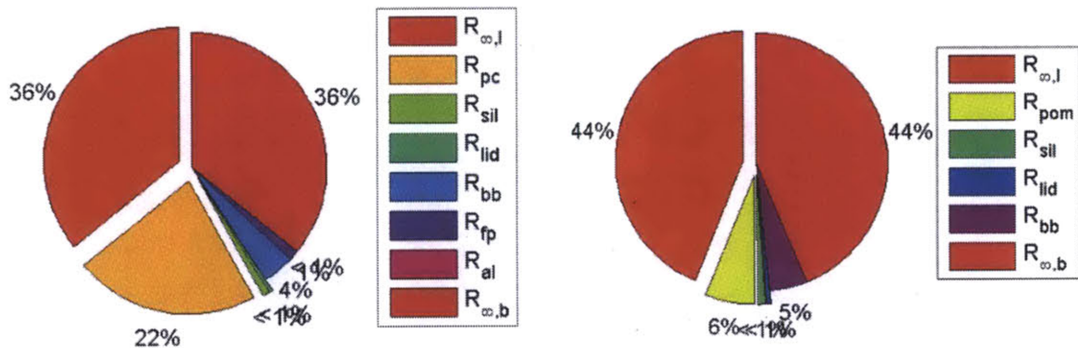

(c) Thermal resistance breakdown of the new fixture

(d) Thermal resistance breakdown of the original fixture

Figure 5-14: A comparison of the thermal resistances of the new versus original fixture in attempt to understand the inability for the new fixture to successfully weld. The lid side R_t''s are exploded on the pie charts

It is qualified that many of the R_t''s are not experienced by the temperature gradient front in short intervals. However, the fact the implants operate at the limit of the minimum heat flux required for bonding is re-emphasized and it is qualitatively demonstrated that thermal resistances are relevant considerations in implant

bonding.

5.4.2 Cuvette Welding Success

Based on the thermal resistances of previous testing and modelling, it was decided that removing material directly under the intended weld area of the new fixture would create an equivalent thermal pathway to the originally successful fixture by having the backbone exposed directly to ambient. However, instead of removing all material underneath the cuvette, an aluminum strip was left precisely underneath the previously documented sensitive channel area (Section 2.3). This material is intended to act as a heat sink that prevents this region of the cuvette from reaching T_{fail} while the bond region should reach T_{bond} only in the immediate vicinity of the conductive implant. If it was shown that complete equivalence to the original fixture was necessary, the heat sink strip could be easily removed with hand tools. The modification is shown in Figure 5-15(c).

It is demonstrated that when all other factors were held constant, the success of welding with the new fixture was entirely dependent on the values of the thermal resistance adjacent to the backbone and lid. While the new fixture has a very skewed HAZ compared to the original according to the steady state $\bar{H}$, this characterization appears less relevant. The resistances immediately "felt" during heating in which steep temperature gradients exist are only those that are adjacent to the lid and backbone. This warrants re-investigating the $\bar{H}$ logic of Section 4.10 in order to accurately incorporate temporal effects and time scales. Nonetheless, the key takeaway is that heating in microfluidic systems is sensitive to thermal resistance values.

With successful welding with the new fixture, more complete weld paths demonstrated a HAZ that prevented black ink from wicking into the volume enclosed. The exterior HAZ that contrasted with the ink is presumed similar to the enclosed section (ink would not flow inside the featureless sample). Iterations of welding parameters can be carried out more quickly and a complete assembly of all of the production components could be implemented. Plumbing was added so that black ink could be manually pumped into the cuvette assembly to highlight the bonded zones. This

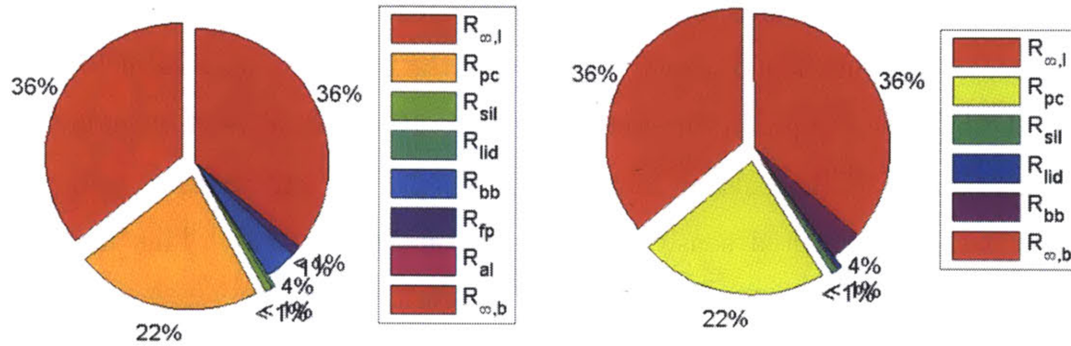

(a) Reprint of new fixture (Figure 5-14(c)) before the modification to expose the backbone to air rather than the fixture

(b) Welding is successful with backbone exposed to ambient R_{∞}, mimicking originally successful fixture

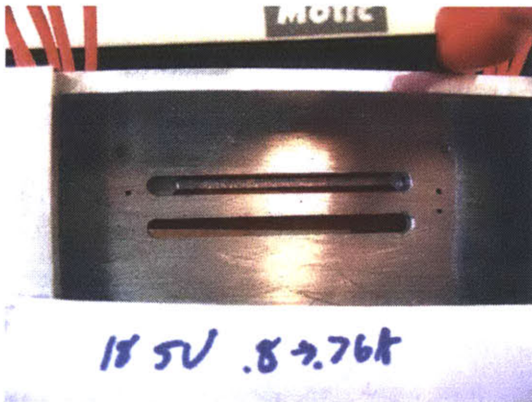

(c) Demonstrated success of modified new fixture with same mock assembly sample (image from fixture underside)

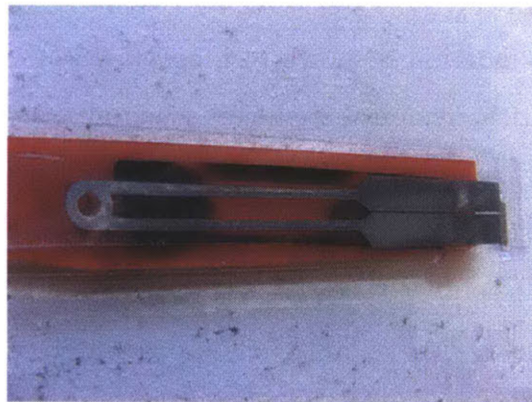

(d) Capillary wicking of ink shows the bonded region on the outside of cuvette, which is presumed representative of the interior

Figure 5-15: Backbone is now directly exposed to the ambient under the implant rather than through an insulator and the fixture. The remaining fixture material acts as a heat sink intended to actively prevent distortion for welding of two sides of the cuvette.

was implemented directly onto the fixture such that a production backbone could be placed in its mount and seal against a gasketed syringe, depicted in Figure 5-16(a).

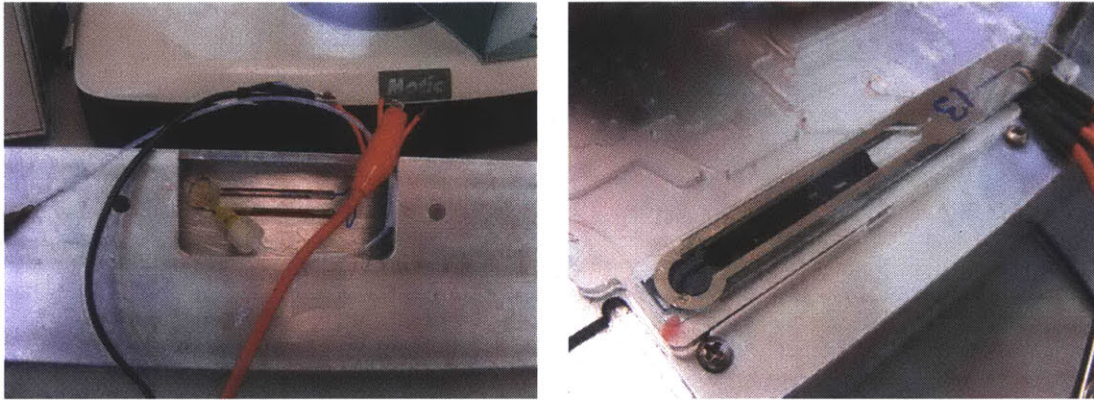

(a) Two sided cuvette bonding and ink test

(b) Ink fills cuvette without overflow within trace boundary

Figure 5-16: Two parallel implants aligned with the new fixture cutouts can bond two sides of the cuvette as testing progresses toward a complete cuvette seal

While testing more complete assemblies, it was discovered that failures due to hot spots were occurring in repeatable locations. This was in contrast with the more random fuse-like failures that could be attributed to uneven pressure, unavoidable differences in thermal expansion, and implant dimensional variability. To confirm that the particular location was an issue, further testing indicated that local hot spots were present since the local R_t'' is much larger. Additionally, failures occurred in the 180 degree semi-circle feature of the same cross section, even though it was positioned over the fixture heat sink. These failures were overcome by thickening the curved section only, indicating that the proximity of the traces to one another effects the total heating and subsequent melting imparted by the implant when the entire bond area is heated at once. Retesting of each correction with the featureless PMMA samples did not reveal any regular failures as discovered when welding the production backbones.

With bonding being accomplished in the new fixture design, parameters can be

optimized to get less cuvette distortion by efficiently creeping up on T_{bond}. While this would create less steep temperature gradients less steep that could be slower overall, the value of distortion-free features shall be weighed against process cycle time. Further testing with completely sealed cuvettes, different welding pressures, optimized heating patterns, or by applying heat with implants from locations other than the intended weld interface may also realize this objective, but would be the subject of future work.

Chapter 6

Executive Summary

The following section summarizes conclusions drawn from the Masters of Engineering in Manufacturing thesis work on *Methods of Heating Microfluidic Components for Assembly* completed between January to August 2012 at Daktari Diagnostics. The paper includes a survey of thermoplastic welding techniques for the demanding cuvette application (Chapters 2 and 3), analysis of PMMA bonding mechanics (Chapter 4), and a proposed method of conductive implant resistive heating (Chapter 5) in an effort to provide recommendations pertaining to cuvette assembly for the Daktari CD4 product. The work demonstrates the feasibility of resistively heating conductive traces in a microfluidic assembly context and well as other "knobs to turn" for further development.

6.1 Synopsis

6.1.1 Cuvette Assembly

While the core technologies of cell chromatography and lysate impedance spectroscopy will enable Daktari to offer resource-limited patients with a CD4 diagnostic product, an optimal design for manufacture is still required. In particular, precise cuvette assembly that recreates ideal assay conditions is critical for accurate diagnostic results. The cuvette channel where the assay occurs has a particularly demanding set of func-

tional requirements compared to other microfluidics in the POC/LOC literature. The pressing challenges at Daktari of controlling fluid flow, fabricating microscale devices out of PMMA, using and storing sensitive solutions in off-the-shelf material, low cost mass manufacture, and the integration of electrical components are not unique among commercial microfluidic platforms. However, designing precise micron scale features conflicts with the low cost constraints for a product marketed for resource-limited settings, necessitating Daktari to invent solutions. In fact, innovations that Daktari implements in their development of the CD4 product are relevant to the entire LOC industry in want of commercially viable solutions, particularly with respect to microfluidic assembly, manipulation, sensing, and temperature cycling.

Thermoplastic microchannels are subject to deformation during joining. At the very least, the deformation causes assemblies to be out of specification, but may also result in assay noise. Furthermore, while the assembly of clear cuvette components would be invaluable to R&D, it is particularly challenging to implement. Alternative solutions must meet performance specifications; ideally the would also be amenable to in-house research and development efforts. Otherwise, proposed solutions must offer another significant advantage as production is scaled such as the reduction of manufacture cycle time, the ability to be automatically QC'd, enhance both process and product capability and robustness, or permit some other advantage for the Daktari business.

6.1.2 Thermoplastic Welding Survey

A survey of mass assembly methods of bonding thermoplastics was conducted, recognizing that a complete homogeneous weld of the cuvette is preferred. Mechanical fasteners may experience leakage if the part experiences runout due to manufacturing limitations or scenarios where ageing, environmental effects, or human handling may disturb the preload.

For non critical components, hot plate and hot wire methods the least expensive methods for immediate microfluidic assembly welding applications. On the other hand, through transmission welding of microfluidics with one micron diode lasers has

been commercially demonstrated for most sensitive microfluidic components, with contour methods being the most flexible for products still in development. Other less serial laser approaches are offered by various vendors and plastic welding solutions are supported by a growing laser welding industry.

Ultrasonic, resistive implant, or inductive welding of microfluidics are the subject of numerous academic studies but are not yet commercially viable for LOC dimensional tolerances. The present work demonstrates that with minimal investment, it is possible to resistively heat conductive implants that are inductively or and physically coupled utilizing components manufactured via Daktari's electrode production process. Said conductive implants can be inspected in quality control with X-rays. Looking forward, ultrasonic and inductive welding may compete with laser welding for high throughput, feature sensitive, and completely non-contact welding. However, both require further development with high initial costs due to the specialized induction and ultrasonic equipment. In comparison to other types of welding, hot plate, hot wire, ultrasonic, and inductively or physically coupled resistive implants create the entire weld seam in parallel that minimizes cycle time once dedicated production machinery is implemented.

6.1.3 Bonding Mechanics Applied to Welding

Bonding Mechanics

PMMA bonding requires energy to be transmitted into the components to be welded such that molecular chain reptation occurs as polymer chains intertwine across the intended weld interface. Thermoplastics have poor thermal diffusivity and thus the PMMA cuvette temperature response is slow in time as heat energy conducts slowly through the thermal bulk. It takes a longer time for PMMA to reach thermal equilibrium than high conductivity materials, and thus very steep temperature gradients exist in the thermoplastic. The thermal conductivity of PMMA is on the order of $10^{-1}\frac{W}{mK}$, while it is 10^{0} and greater than $10^{1}\frac{W}{mK}$ for glasses and metals, respectively. Additionally, PMMA has a 10 times higher coefficient of thermal expansion compared

to some non-plastic materials, indicating that stresses may develop due to dissimilar expansion rates during heating. Increasing the pressure during welding of the components decreases the amount of energy required to produce a bond, but must be balanced against the resiliency of the cuvette to clamping forces.

A simplified thermal resistance model of energy being added to the cuvette directly to the intended weld interface is created. The model indicates a minimum heat flux rate, q''_{min} for PMMA bonding for the steady state condition when thermal and temporal gradients have ceased after significant time has elapsed. Additionally, the importance of the thermal resistance (R''_t) values of the cuvette welding system is highlighted, especially with respect to the required energy sensitivity to the embodied fixture, contact resistance from air gaps, and the resultant weld heat-affected zone. There is a potential opportunity to engineer an asymmetric HAZ in order to bias melting and deformation towards the less-sensitive lid side of the cuvette assembly by tuning the thermal resistances of the weld fixture. Considering non-equilibrium heating, it is reaffirmed that the PMMA cuvette will have steep thermal gradients within the mass as well as in time. However, the non-linear and inter-related dynamic rates of change of the material properties and other instantaneous weld state are very difficult to characterize in closed form. Advanced simulation would be required to correlate the measured response of the weld system's temporal and spatial thermal gradients.

6.1.4 Heating Thin Implants

Daktari has a flexible and robust sensing electrode production process. The same process can accurately produce implant patterns for resistive heating with electric current from either inductive coupling or physical contact and continuity to an electric power source. While the opportunity of inductive coupling was explored prior, simple DC resistive heating could more efficiently validate the feasibility of heating thin implants in the cuvette as a welding process with very simple equipment and knowledge of basic electrical phenomenon. In addition, the welds from the implants occur safely within the line of sight of the practitioner for optical observation or

non-contact thermographic recording.

In short order, testing by connecting implants directly to a power supply validated the efficacy of heating the electrode material to the melting temperatures of PMMA. The material actually demonstrated sustaining current densities (and thus power levels) surpassing manufacturer ratings. It should be noted that the material properties disclosed by the manufacturer are minimal and it is difficult to characterize potential operational sensitivities to the sourced material variation.

Further high current heating experimentation with the material indicated that it could sustain about $3W$ for a qualitatively significant period. Unlike a perfect resistor, temperature of the implant increases with time, causing the material resistivity to increase and thus reduce the instantaneous heater power output when a fixed voltage potential was supplied. Preliminary data of theses phenomenon were captured and plotted, indicating first order correlations that may be used in developing sensors that relate system state values (such as temperature) to electrical signals for sensors. Though it was not possible to get a completely accurate temperature reading during testing due to thermocouple location and thermal response, heating rates were recorded to be at least $0.5\frac{^oC}{s}$. Successful welds always took place in under 5 minutes, with weld times of about 1 minute sporadically occurring, barring premature implant failure. The testing of this study did not otherwise test explicitly for potential cuvette assembly cycle times. Manual peels tests on welds produced on clear PMMA featureless backbone samples tore in the production lid material rather than at the weld, indicating complete polymer reptation is possible with thin implant welding.

The welding success of the initial fixture turned out to be coincidental, because a more specifically designed resistive implant welding fixture at first failed to bond identical samples. Recalling the potential sensitivity to the fixture R_t'', especially since the resistive implant power levels are presumed lower than that the laser capability, the fixture was reworked to be R_t'' equivalent to the initial fixture. High R_t'' values were introduced directly adjacent to the intended implant weld line, while the predicted fixture heat sink remained directly abutting the cuvette channel to reduce thermal build up and hopefully deformation. Subsequent testing confirmed the

designed welding fixture's sensitivity to R_t''s and faster design iterations could occur with more ambitious implant patterns and production backbones. With more repeatable bonding, further testing identified continuity-severing failure locuses at hotspots along the trace. These are presumed to be nominally the result of material defects or implant/PMMA thermal expansion differences stressing the implant during heating, changing the trace cross sectional area, thus increasing the current density such that thermal runaway ensues. Additionally, unanticipated heating of production components from the proximity of traces to one another as well as additional R_t'' added by air trapped in channels on the opposite fluidic side of the backbone resulted in hotspots and even sparking with fuse-like failures. Fortunately, the flexible method of producing conductive implants permits rapid design iterations and many of the discernible failures quickly had engineering solutions for the successful welding of a clear PMMA production cuvette that withstood the manual pumping of ink on the two long sides of the channel.

Due to inadequate data collection beyond initial tests of feasibility, most resistive implant welding parameters are not accurately quantifiable to any certainty. However, the theoretical work-up of the cuvette welding method is outlined for subsequent work based on the demonstrated preliminary success. This future work will have a profound materials section, an experimental hard labor component, and require partnership with the manufacturer to make resistive heating of conductive traces a reality in microfluidics [22]

Bibliography

[1] Aaron Oppenheimer. DaktariDx.com. *Company Website*, 2012.

[2] Joint United Nations Program on HIV/AIDS. World AIDS Day Report. *UN-AIDS*, 2011.

[3] Tim Horn. What is AIDS & HIV? *AIDSMEDS*, 2012.

[4] Michael Carter and Greta Hughson. CD4 Cell Counts. *NAM Publications*, 2012.

[5] United States Government. What is HIV/AIDS?, June 2011.

[6] W. Rodriguez, M. Toner, and Et Al. A microchip approach for practical label free CD4+ T-cell counting of HIV infected subject in resource poor settings. *Journal of Acquired Immune Deficiency Syndrome*, 45(3):251–261, 2007.

[7] WHO. Progress on Global Access to HIV Antiretroviral Therapy: An update on "3 by 5". *World Health Organization*, June, 2005.

[8] Paul Yager, Thayne Edwards, Elain Fu, Kristen Helton, Kjell Nelson, Milton R Tam, and Bernhard H Weigl. Microfluidic diagnostic technologies for global public health. *Nature*, 442(7101):412–8, July 2006.

[9] R Zengerle. Microfluidic Platforms for Lab on a Chip Applications. *Lab on a Chip*, 7(9):1094–1110, 2007.

[10] V. Liner. Microfluidics at the Crossroads of Diagnostics. *The Analyst*, 132:1186–1192, 2007.

[11] Yi Ter Ter. Creating Microfluidic Devices: The Future for Point of Care Diagnostics. *Basic Biotechnology eJournal*, 3(9):40–46, 2007.

[12] Patrick Tabeling. Introduction to Microfluidics. *Angewandte Chemie*, 118(47):8039–8040, 2006.

[13] S. Selvakumar. *Manufacturing of Lab-on-a-Chip Devices: Variation Analysis of Liquid Delivery using Blister Packs.* Masters of engineering, MIT, 2010.

[14] Xuanhong Cheng, Daniel Irimia, Meredith Dixon, Kazuhiko Sekine, Utkan Demirci, Lee Zamir, Ronald G Tompkins, William Rodriguez, and Mehmet Toner. A microfluidic device for practical label-free CD4(+) T cell counting of HIV-infected subjects. *Lab on a chip*, 7(2):170–8, February 2007.

[15] Xuanhong Cheng, Yi-shao Liu, Daniel Irimia, Utkan Demirci, Liju Yang, Lee Zamir, William R Rodríguez, Mehmet Toner, and Rashid Bashir. Cell detection and counting through cell lysate impedance spectroscopy in microfluidic devices. *Lab on a chip*, 7(6):746–55, June 2007.

[16] Nikhil Jain. *A Comprehensive Study and Validation of High-Throughput Microscale Electrode Production.* Meng thesis (in preparation), Massachusetts Institute of Technology, 2012.

[17] Tejas Inamdar. *Manufacturing of Lab-on-a-Chip Devices: Characterizing Reagent Delivery Using Blister Packs.* Meng thesis (in preparation), Massachusetts Institute of Technology, 2012.

[18] Aabed Saber. *Manufacturability of Lab on Chip Devices: Blister Pack Production Process and its Effect on Performance.* Meng thesis (in preparation), Massachusetts Institute of Technology, 2012.

[19] L. Donoghue. *Design of a Micro-Interdigitated Electrode for Impedance Measurement Performance in a Biochemical Assay.* Meng thesis, MIT, 2011.

[20] Linear Polydimethylsiloxanes. *Joint Assessment of Commodity Chemicals*, 26(September), 1994.

[21] LILY. Interview with Melinda Hale: Low-cost manufacturing of microfluidic devices. *FluidicMEMS: Perspectives on LOC, Microfluidic, and BioMEMS Technology*, October 2010.

[22] Robert Etheredge. Personal Conversations, 2012.

[23] CD Chin and V Linder. Commercialization of microfluidic point-of-care diagnostic devices. *Lab Chip*, (207890), 2012.

[24] Yager, P. Microfluidic Diagnostics Technolgoies for Global Public Health. *Nature2*, 442(7101):412–8, 2006.

[25] M. Czugala, B. Ziolkowski, R. Byrne, D. Diamond, and F. Benito-Lopez. Materials science: the key to revolutionary breakthroughs in micro-fluidic devices. *Library*, 8107:81070C–81070C–10, 2011.

[26] Jason S Kuo and Daniel T Chiu. Disposable microfluidic substrates: transitioning from the research laboratory into the clinic. *Lab on a chip*, 11(16):2656–65, August 2011.

[27] Pedro S. Nunes, Pelle D. Ohlsson, Olga Ordeig, and Jörg P. Kutter. Cyclic olefin polymers: emerging materials for lab-on-a-chip applications. *Microfluidics and Nanofluidics*, 9(2-3):145–161, April 2010.

[28] Chia-Wen Tsao and Don L. DeVoe. Bonding of thermoplastic polymer microfluidics. *Microfluidics and Nanofluidics*, 6(1):1–16, November 2008.

[29] Dennis Patrick Webb, Benedikt J. Knauf, Changqing Liu, and D Hutt. Productionisation issues for commercialisation of microfluidic based devices. *Sensor Review*, 2009.

[30] Benedikt J. Knauf, Dennis Patrick Webb, Changqing Liu, and Paul P. Conway. Low frequency induction heating for the sealing of plastic microfluidic systems. *Microfluidics and Nanofluidics*, 9(2-3):243–252, November 2009.

[31] R J Wise. Thermal Welding of Polymers. Technical report, Abington Publishing, Cambridge, 1999.

[32] BASF. Snap-Fit Design Manual. Technical report, 2007.

[33] Ulrich A. Russek. *Laser Welding of Polymers.* Suddeutscher Verlag onpact GmbH, Munich, 2009.

[34] Jordan Rotheiser. *Joining of Plastics.* Hanser Gardner, Inc, Munich, 2 edition, 2004.

[35] Hot Gas Welding. *Welding Machines Information and Review*, June 2012.

[36] Patrick Abgrall, Lee-Ngo Low, and Nam-Trung Nguyen. Fabrication of planar nanofluidic channels in a thermoplastic by hot-embossing and thermal bonding. *Lab on a chip*, 7(4):520–2, April 2007.

[37] Jesse Greener, Wei J. Li, Judy Ren, Dan Voicu, Viktoriya Pakharenko, Tian Tang, and Eugenia Kumacheva. Rapid, cost-efficient fabrication of microfluidic reactors in thermoplastic polymers by combining photolithography and hot embossing. *Lab on a chip*, 10(4):522–4, February 2010.

[38] Xia Wang, Luyan Zhang, and Gang Chen. Hot embossing and thermal bonding of poly(methyl methacrylate) microfluidic chips using positive temperature coefficient ceramic heater. *Analytical and bioanalytical chemistry*, 401(8):2657–65, November 2011.

[39] Bob Mileti. Trlby Innovative, LLC, 2012.

[40] Roman Truckenmüller, Y. Cheng, R. Ahrens, H. Bahrs, Günther Fischer, and J. Lehmann. Micro ultrasonic welding: joining of chemically inert polymer microparts for single material fluidic components and systems. *Microsystem Technologies*, 12(10-11):1027–1029, April 2006.

[41] Roman Truckenmüller, Ralf Ahrens, Yue Cheng, Günther Fischer, and Volker Saile. An ultrasonic welding based process for building up a new class of inert fluidic microsensors and -actuators from polymers. *Sensors and Actuators A: Physical*, 132(1):385–392, November 2006.

[42] Zongbo Zhang, Yi Luo, Xiaodong Wang, Yingsong Zheng, Yanguo Zhang, and Liding Wang. A low temperature ultrasonic bonding method for PMMA microfluidic chips. *Microsystem Technologies*, 16(4):533–541, January 2010.

[43] Jongbaeg Kim, Bongwon Jeong, and Mu Chiao. Ultrasonic bonding for MEMS sealing and packaging. *Advanced Packaging, IEEE*, 32(2):461–467, 2009.

[44] Yi Luo, Zongbo Zhang, Xiaodong Wang, and Yingsong Zheng. Ultrasonic bonding for thermoplastic microfluidic devices without energy director. *Microelectronic Engineering*, 87(11):2429–2436, November 2010.

[45] S.H. Ng, Z.F. Wang, and N.F. de Rooij. Microfluidic connectors by ultrasonic welding. *Microelectronic Engineering*, 86(4-6):1354–1357, April 2009.

[46] Yibo Sun, Yi Luo, Xiaodong Wang, Miaomiao Zhang, and Yuqi Feng. A new ultrasonic precise bonding method with ultrasound propagation feedback for polymer MEMS. *Microelectronic Engineering*, 88(10):3049–3053, October 2011.

[47] Induction Atmospheres. The Induction Heating Guide. Technical report, 2010.

[48] S Christensen. Structural susceptor for thermoplastic welding. *US Patent 5,717,191*, 1998.

[49] KA Hansen. selvaged susceptor for thermoplastic welding by induction heating. *US Patent 5,508,496*, 1996.

[50] V. a. Kagan. Benefits of Induction Welding of Reinforced Thermoplastics in High Performance Applications. *Journal of Reinforced Plastics and Composites*, 24(13):1345–1352, September 2005.

[51] EA Riess, AG Malofsky, and JP Barber. Method of adhesive bonding by induction heating. *US Patent 6,849,837*, 2005.

[52] WO Patent WO/2010/033, 163 and 2010. ELECTROMAGNETIC BOND WELDING OF THERMOPLASTIC PIPE DISTRIBUTION SYSTEMS. *wipo.int*.

[53] A DIY Induction Heater, 2012.

[54] OpenSchemes. Circuit analysis of the 1.8kW Induction Hotplate, 2010.

[55] V Nemkov and R Goldstein. Optimal Design of Internal Induction Coils. *Heat Treating Progress*, (1), 2005.

[56] RJ Nichols and DP LaMarca. Performance of susceptor materials in high frequency magnetic fields. *Proceedings of ANTEC, SPE*, (8):1–5, 2006.

[57] D Puyal and C Bernal. Methods and procedures for accurate induction heating load measurement and characterization. *Electronics, 2007. ISIE*, pages 805–810, 2007.

[58] Stanley Zinn. Coil design and fabrication: basic design and modifications. *Heat Treating*, (June), 1988.

[59] Benedikt J. Knauf. Polymer Bonding by Induction Heating for Microfluidic Applications. *Loughborough University PhD Thesis*, 2010.

[60] Benedikt J. Knauf, Dennis Patrick Webb, and Changqing Liu. *Low frequency induction heating for the sealing of plastic microfluidic systems.* PhD thesis, Loughborough, 2010.

[61] Benedikt J. Knauf, Dennis Patrick Webb, and Changqing Liu. Packaging of polymer based microfluidic systems using low frequency induction heating (LFIH). *Electronic Packaging*, 2008.

[62] Benedikt J. Knauf, Dennis Patrick Webb, Changqing Liu, and Paul P. Conway. Plastic Packaging Using Low Frequency Induction Heating (LFIH) For Microsystems. *2008 10th Electronics Packaging Technology Conference*, pages 172–180, December 2008.

[63] Garrett Churchhill. Powerful Induction Heating You Can Afford, 2012.

[64] Emabond Solutions. Superior Plastic Welds for Demanding Applications. July 2012.

[65] Dynamic Manufacturing Solutions. Dielectric Welding. *DMS*, June 2012.

[66] T; Meister J Labuza. An alternative method for measuring the heating potential of microwave suseptor films. Technical report, International Microwave Power Institute, 1988.

[67] P M Harms, Y Chen, R Mittra, and Y Shimony. Numerical Modeling of Microwave Heating Systems. *Journal Of Microwave Power*, 21(2):99–124, 2010.

[68] Kin Fong Lei, Syed Ahsan, Nasser Budraa, Wen J. Li, and John D. Mai. Microwave bonding of polymer-based substrates for potential encapsulated micro/nanofluidic device fabrication. *Sensors and Actuators A: Physical*, 114(2-3):340–346, September 2004.

[69] Krishnamoorthy Pitchai. Modeling of Susceptor Assisted Microwave Heating in Domestic Ovens. In *Electromagnetic Heating*, 2011.

[70] Michelle E Lustrino. *The Development of an Innovative Bonding Method for Microfluidic Applications.* Sm thesis, MIT, 2011.

[71] F Bundgaard, G Perozziello, and O Geschke. Rapid prototyping tools and methods for all-Topas cyclic olefin copolymer fluidic microsystems. *Proceedings of the Institution of Mechanical Engineers, Part C: Journal of Mechanical Engineering Science*, 220(11):1625–1632, January 2006.

[72] Mike Ashby and Kara Johnson. *Materials and Design: The Art and Science of Material Selection in Product Design.* Butterworth-Heinemann, Boston, 1 edition, 2002.

[73] Frank Incropera and David DeWitt. *Fundamentals of Heat and Mass Transfer.* John Wiley & Sons, Hoboken, 5th edition, 2002.

[74] Mingliang Chen, Gene Zak, and Philip J. Bates. Effect of carbon black on light transmission in laser welding of thermoplastics. *Journal of Materials Processing Technology*, 211(1):43–47, January 2011.

[75] Anne Mäntymaa, Jussi Halme, Lasse Välimaa, and Pasi Kallio. The effects of laser welding on heterogeneous immunoassay performance in a microfluidic cartridge. *Biomicrofluidics*, 5(4):46504–4650411, December 2011.

[76] Pyshar Yi, Aminuddin a. Kayani, Adam F. Chrimes, Kamran Ghorbani, Saeid Nahavandi, Kourosh Kalantar-zadeh, and Khashayar Khoshmanesh. Thermal analysis of nanofluids in microfluidics using an infrared camera. *Lab on a Chip*, 2012.

[77] Joao M. P. Coelho, Manuel a. Abreu, and F. Carvalho Rodrigues. Modeling CO[sub 2] laser radiation transmission lap welding of thermoplastic films: energy balance approximation. *Optical Engineering*, 46(6):064301, 2007.

[78] E Haberstroh and W-M Hoffmann. Laser transmission welding of complex micro plastic parts. *Proceedings of the Institution of Mechanical Engineers, Part B: Journal of Engineering Manufacture*, 222(1):47–54, January 2008.

[79] Friedrich G Bachmann and Ulrich A Russek. Laser Welding of Polymers Using High Power Diode Lasers ROFIN-SINAR Laser GmbH ; b Fraunhofer-Institute for Laser Technology. 49(0).

[80] James D. Van de Ven and Arthur G. Erdman. Bridging Gaps in Laser Transmission Welding of Thermoplastics. *Journal of Manufacturing Science and Engineering*, 129(6):1011, 2007.